McGill STRUCTURES AND COMPOSITE MATERIALS LABORATORY

Secondary Bonded Pi-Joint Out of Autoclave Process

By

Navid Ghomi, October 2013

Structures and Composite Materials Laboratory

Department of Mechanical Engineering

McGill University, Montreal

A thesis Submitted to McGill University

In partial fulfillment of the requirements of the degree of

Masters in Engineering

Abstract

Composite materials are widely used in the aerospace industry due to their high strength and stiffness properties, as well as the manufacturing possibilities they offer for large components at lower assembly costs. To further lower the manufacturing cost, the use of Out of Autoclave (OOA) process is increasing in popularity. However, mechanically joining parts is a necessary step in the assembly of a large component, driving up the weight of the component and the final assembly cost. A Pi-Joint is one way to offer lower assembly cost through secondary bonding while ensuring the joint's reliability due to the redundancy in the load path. Predicting the failure strength of a bonded joint is essential for the initial stages of aircraft structure design. In this research project, the OOA process is used to manufacture Pi-Joints using pre-impregnated carbon fibre fabric. The Pi-Joint is co-cured with the skin, followed by a secondary bond operation of the web onto the Pi-Joint and skin assembly. To assess the strength of the joint, four different manufacturing techniques are used. In addition, a finite element analysis technique is used to estimate the first mode of failure for the different configurations of the Pi-Joint. The failure strength is correlated with experimental test results to determine the reliability of the manufacturing techniques. Static strength analyses are carried out along with mechanical tests to assess the redundancy of the load path. It is shown in this research that the finite element modelling results are in agreement with the test results.

Résumé

Les matériaux composites sont largement utilisés dans l'industrie aéronautique en raison de leur grande résistance, de leur rigidité, et de leur facilité à être fabriquée en composantes de grandes dimensions à faible coût. Afin de minimiser d'avantage les coûts liés à la fabrication des pièces, le processus de fabrication hors autoclave ou OOA est de plus en plus utilisé. Cependant, l'assemblage mécanique des pièces constitue une étape inévitable de l'assemblage du produit. Ce processus a pour effet d'augmenter le poids et le coût de l'assemblage final. L'utilisation du Joint en Pi qui assemble la structure par un collage secondaire permet de réduire les coûts et d'augmenter la fiabilité du produit final grâce à la multiplicité des chemins de charge qu'il offre. Prédire la défaillance d'un joint collé est essentielle aux phases préliminaires de design des structures primaires d'un avion. Dans ce projet de recherche, le procédé OOA est utilisé afin de fabriquer des joints en composite à base de fibre de carbone. Le Joint en Pi est cocuit avec le revêtement puis une cuisson secondaire permet de joindre l'âme à l'assemblage du Joint en Pi et du revêtement.

Afin de déterminer la rigidité du joint, quatre techniques de fabrication sont utilisées. De plus, des analyses par éléments finis sont utilisées afin de prédire le premier mode de défaillance pour diverses configurations du Joint en Pi. La résistance à la défaillance est corrélée avec des résultats de tests expérimentaux afin d'assurer la fiabilité du procédé de fabrication. Des analyses statiques et des tests sont réalisés afin de démontrer la multiplicité du chemin de charge. Dans cette recherche il est montré que les résultats des analyses par élément finis sont en accord avec les résultats des tests.

Acknowledgements

I wish to express my sincere gratitude to my supervisor, Dr. Pascal Hubert, for giving such a great opportunity to be a member of his research group and providing me with the opportunity to work in such dynamic environment. He is an admirable person of great knowledge and experience and I am truly grateful for his immense guidance and support throughout my study.

It is paramount to mention the partners in this project: Bombardier Aerospace, Bell Helicopter Textron Canada, Delastek Inc., the Centre for the Development of Composites of Québec (CDCQ), the Consortium for Research and Innovation in Aerospace in Québec (CRIAQ), the National Research Council of Canada (NRC), the Center for Applied Research on Polymers (CREPEC) and NSERC, specifically to Bombardier Aerospace and Bell Helicopter for providing the materials and essentials.

I would like to thank Melanie Brillant, Jim Kratz and Timotei Centea for their assistance on proper use of the equipment at the lab. I would like to acknowledge and appreciate the welcoming and dynamic work environment and the lab mates at the Structures and Composite Materials Laboratory at McGill for their meaningful discussions and assistance.

Last, but not least, I would like to express my appreciation to my family for their generous encouragements throughout my studies, specially my wife Dr. Mahsa Hamzeh and my sweetheart Aiden D. Ghomi.

Table of Contents

List of Tables

List of Figures

Chapter 1.

Introduction

1.1. Aerospace Industry and Composites

Due to their superior mechanical performance, composites are used extensively in commercial and military aircrafts. In order to apply the knowledge and the technology developed for composites to the aerospace industry, Boeing in collaboration with NASA, initiated Advanced Technology Composite Aircraft Structures (ATCAS), in May 1989. The goal of the ATCAS program was to develop the technology required for the cost and weight efficient use of composites in commercial transport [1]. The target was to develop composite structures for commercial transport with 20- 25% less cost and 30-50% less weight than equivalent metallic structures [2].

The material chosen for the ATCAS program was carbon fibre reinforced epoxy. The process chosen was the automated fibre placement for both monolithic and sandwich panels. For the frames, resin transfer molding was chosen. Pultrusion was chosen for floor beams and constant section stiffeners. Drape forming was chosen for stringers and other stiffeners [1]. The ATCAS program paved the way for the use of composite primary structures in commercial airplanes.

The Dreamliner Boeing 787, see Figure 1,uses up to 50% composite materials [3], the Airbus A350 XWB airframe contains at least 53 % of carbon fibre composites [4] and Learjet 85 fuselage, vertical stabilizer, horizontal stabilizer, and wing are built primarily from carbon composites.

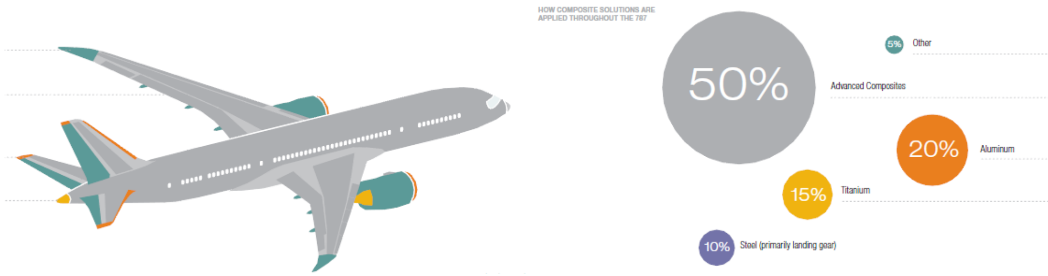

Figure 1 Boeing 787 percentage of composite used in the primary structure [3]

Due to cost and simplicity of the manufacturing techniques thermosets are preferred over thermoplastics for aerospace applications.

1.2. Composite Mechanical Joints versus Bonded Joints

1.2.1. Composite Mechanical Joints

To join two parts together mechanically, the parts must be drilled first and then attached together with fasteners. By creating holes, stress concentration is generated in the part. As it is shown in Figure 2, stress concentration due to the circular hole for a typical orthotropic material can be as high as 8.0.

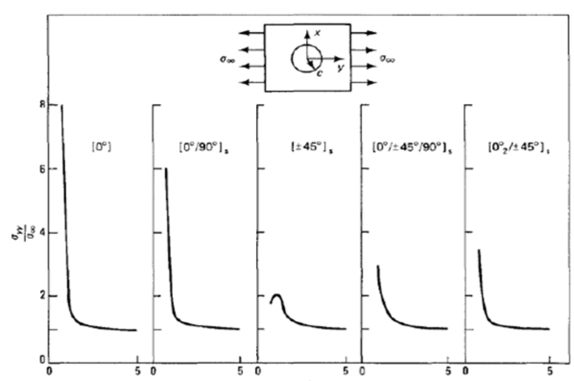

Figure 2 Stress concentration factor for a circular hole in a homogeneous, orthotropic infinite plate [5]

Thus, depending on the layup near the fastener, the part must locally be reinforced. This is neither cost nor weight efficient. Therefore, adhesive bonding can potentially eliminate the stress concentration around the holes and the costly operation of mechanically jointing two parts together [6].

On the other hand, the most important advantage of mechanically fastening joints is the reliability and redundancy in the load path. If one fastener is loosened, for example because of the lost in the pretension load, the ability to transfer the load between two parts at that fastener is lowered. However, in a multi-load path joint (multiple fasteners); the load will redistribute itself to adjacent fasteners and the total load is transferred.

The shear strength of the joint is predicted by the minimum strength of one of the following failure modes [7]:

1. Bearing bypass strength of the adherent in the laminate.
2. Bearing strength of the adherent.
3. Shear-out strength of the adherent.
4. Net-tension strength in the laminate.
5. Shear strength of the fastener.
6. Axial strength of the fastener.
7. Pin bending of the fastener.

All these failure modes are well predicted with tests and they are repeatable, considering statistical variations.

1.2.2. Composite Bonded Joints

The main concern with bonded joints is the reliability and the prediction of the bond-line strength. Multi-load path is one way to ensure the redundancy in the load path and being able to detect strength degradation in the joint before catastrophic failure of the bond-line. The simplest approach is to have a joint that is designed with dual load path and each load path is able to carry the limit load independently. Two load paths are able to carry ultimate load and a failure of one load path is independent to the other. Therefore, this joint is a multi-load path and fail-safe design [8]. The other important issue to consider about bonded joints is the direction of load transfer. Usually adhesives have superior shear strength compare to tension strength. The design must be such to ensure the load transfer is only shear load under different loading conditions of the structure. Double lap joint is an excellence example of shear load transfer. Moreover, it is imperative to minimize peel stress in the bonded joints due the limited peel strength in the bond-line. There are many ways to reduce the peel stress in the bonded joint such as:

1. Tapering down the end of the parts to increase the flexibility of the parts where the peel stress is at maximum such as tapered single-lap joint, see Figure 3.
2. Double shear lap joint or minimizing eccentricity in the load transfer such as tapered single-lap joint, see Figure 4.

Figure 3 Tapered single-lap joint [12]

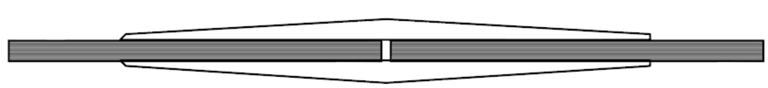

Figure 4 Tapered Double-lap joint [12]

A reliable bonded joint design must inherit the reliability of mechanically fastened joints with the weight saving and cost efficiency. Pi-Joint is an example of bonded joint, see Figure 5.

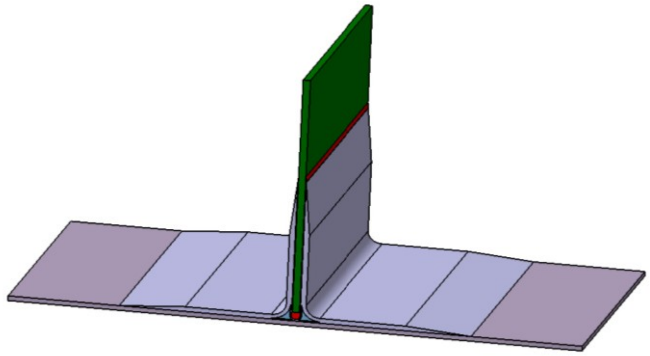

Figure 5 Bonded Pi-Joint

The independent multi load path and reduced peel stress in the joint insures the reliability of Pi-Joints. Of course, it is essential to co-cure the preformed Pi section to the skin. Repeatability of the process is a challenging task and it will be addressed later on in the thesis.

Moreover, a major weight saving can be obtained by evaluating the overall design feature's rather than by optimizing parts locally. Pi-Joint advantages are summarized below [20]:

1. Redundancy in the load path.
2. Two independent bond-lines.
3. High shear properties of the adhesive material.
4. Considerable reduction in assembly time and cost.
5. Adhesive out time is minimal with the Pi-Joint.
6. Less time to apply the adhesive into the clevis of the Pi-Joint.
7. Less surface area is exposed to the air before bonding takes place, lower chance of contamination.
8. No stress concentration around fastener holes compared to mechanically fastened joints.

1.3. Out-of-Autoclave versus Autoclave Manufacturing

1.3.1. Autoclave Manufacturing

An autoclave is a pressure vessel with a heating system, whereas the oven is not equipped with the capability to apply or control pressure. The temperature, pressure and vacuum cycle in the autoclave affect the final part quality of a part in terms of mechanical properties, void content, warpage, thickness variation, fibre to resin ratio [9].

The advantage of an autoclave cure is having a repeatable and controlled process, resulting in components with the desirable high fibre volume fraction. However, the initial investment associated with the autoclave cost and the high operating costs are some of the downsides of using the autoclave cure method. Moreover, the size of the autoclave is a restriction on the size of the part being cured. Large autoclaves are exponentially more expensive [9]. A typical autoclave cure cycle is shown in Figure 6.

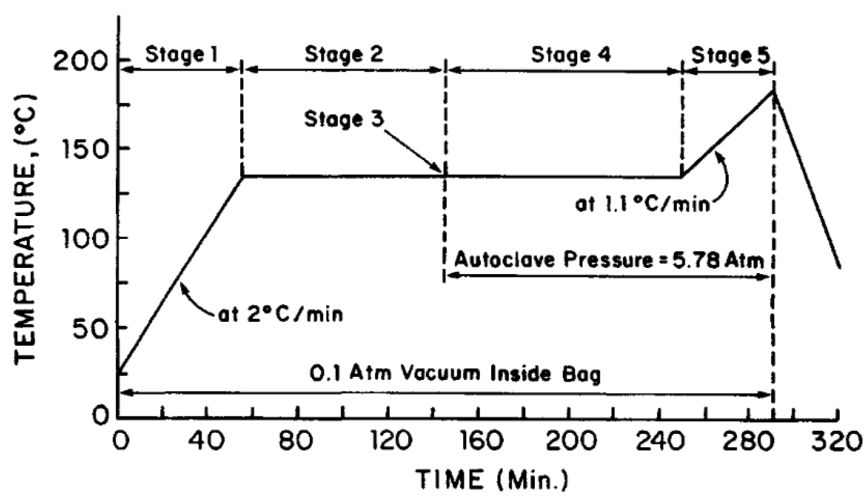

Figure 6 Typical curing cycle temperature-time profile for graphite-epoxy composite in autoclave process [10].

1.3.2. Out-of-Autoclave Manufacturing

Out-of-Autoclave (OOA) manufacturing of composites is an innovative method that has been considered as a replacement to autoclave cures due to its capability to reduce the capital expense for the manufacturing of aerospace-grade structures [11]. The OOA cure process eliminates the high pressure application and introduces atmospheric pressure limited to the vacuum bag pressure to ensure the consolidation of the resin and fibres. The upper and lower portion of the prepreg is partially impregnated with the resin creating a dry porous medium in the middle of the prepreg to enable the evacuation of any entrapped air before the resin becomes liquid and wet the dry fibres [9], see Figure 7. This feature of the pregreg increases the prepreg's ability to bleed the air entrapped during the layup process or the created volatiles during the processing and chemical reactions.

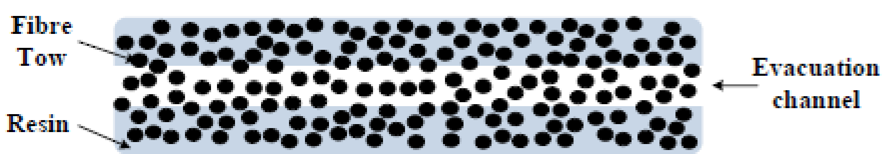

Figure 7 Prepreg CYCOM 5320-1 Epoxy Resin System [22]

It is important to ensure that resin is held at a low viscosity point for a long time to allow for all the fibres to be wetted. Typically, an OOA cure cycle is considerably longer than an autoclave cure cycle to ensure the extraction of the air and volatiles from the laminate and wetting of all dry fibres.

1.4. Pre-Formed Bonded Pi-Joint

In 2006, John D. Russell presented the use of bonded Pi-Joints in primary structure using the Vacuum Resin Transfer Molding manufacturing process. The goal was to certify a large component with integrated stiffeners and bonded primary structures [13]. Structural testing of a full-scale F-35 replica wing, vertical tail and X-45 replica wing was performed to assess the Pi-Joint design feature integrated in these structures[13]. Some of the advantages for bonded Pi-Joint design were:

1. Pi-Joints bonded onto a structure using paste adhesive at room temperature cure are stronger than those co-cured with the structure.
2. A Pi-Joint is not the weak link in a primary structural application.
3. A Pi-Joint is tolerant of several defects such as bondline thickness variation between the web and the preformed Pi (the bondline thickness might not be greater on each side on the web compare to the other side), other manufacturing defects such as voids and peel plies that were not removed prior to bonding.
4. By attaching a Pi-Joint to the structure with adhesive rather than mechanically joining it to the structure with fasteners; the assembly time can be reduced by 50-80% depending on the component, translating to a considerable reduction in cost.
5. Moreover, the assembly time of web to the skin is reduced even more because the geometry of the Pi-Joint compared to a typical bonded joint. Since the preformed-Pi is acting as alignment tool, placing the web into the preformed-Pi does not require any special procedure or tool.

Figure 8 shows the Pi-Joint that was studied as part of Composite Affordability Initiative (CAI).

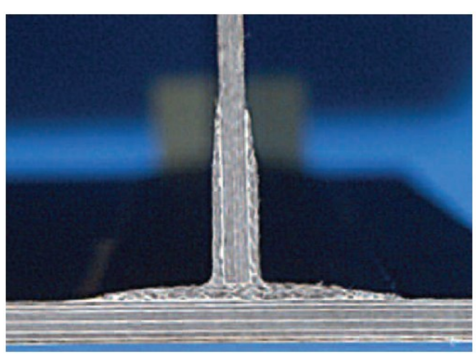

Figure 8 Cross section of the Pi-joint studied in CAI [13]

In 2008, Collier et al carried out research design on a full-scale composite crew module which incorporates bonded joint design features extensively [14]. Preformed Pi-Joints were used to attach the backbone to the lobed dome, and the gusset plate to the pressure shell tunnel and ceiling [14]. The Pi-Joints were bonded in an out-of-autoclave cure [14]. A building block test program was performed to provide the pull-off and shear strength of the joint [14].

In 2009, Zhao et al examined the mechanical performance and estimated the strength of the Pi-Joint using 3D finite element modelling [15]. It was shown that the majority of the load is transferred from the web to the skin through the radius of the L-Segment and the filler. During the mechanical testing, the failure load was determined conservatively as the first mode of failure of the joint. It was also shown in the study that the filler is the weakest point in the joint [15].

In 2010, Tserpes et al studied the effect of imperfect bonding on the pullout behaviour of Pi-Joints. A simplified engineering approach for evaluating the behaviour of Non Crimp Fabric, NCF, given the homogenized behaviour of the constituent layers was presented in their research study. A mesomechanical model was used to predict the pullout behaviour of the Pi-Joint. [16]. A reduction in joint stiffness had a considerable effect on the load increase. Moreover, an ultrasound inspection technique was used to assess the quality of the bond between the pre-formed Pi and the web. A significant amount of voids was detected in the specimens leading to a small reduction in pullout strength [16]. Ultimately the voids had a minimal influence in the load-carrying capability of the joint. Numerical results for failure mechanisms and failure loads were in good agreement with experimental results [16].

In 2010, Zhao et al investigated the behaviour of an all-composite Pi-Joint under a static tensile load [17]. The main research objectives were as follow [17]:

1. To accurately predict the structural stiffness and strength of a composite Pi-Joint.

2. To identify the failure mechanisms of joint.
3. To outline the location and sequence of failure inception.
4. To define the progression of damage up to ultimate collapse in the joint structure.
5. To characterize the stress patterns and load transfer paths in the composite Pi-Joint under the applied load and partial failure conditions.

The study was focused on the damage onset, damage propagation, and ultimate collapse of the composite Pi-Joint simulated by a progressive damage method. The numerical results included [17]:

1. The initial and final failure loads, the failure mode and extent of damage.
2. The stress distribution at a given load.
3. The failure progression.
4. Failure pattern from initial loading to final failure.

It was demonstrated that the numerical predictions are in-line with experimental results [17].

In 2010, Kapoor1 et al carried out a study to detect damage in constrained geometries like z-pinned structured, see Figure 9, and co-cured composite Pi-Joints using ultrasound and scanning laser vibrometry measurements [18].

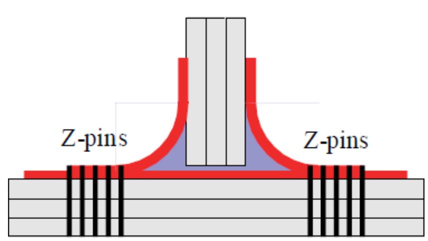

Figure 9 Z-Pinned Joint Reinforcement [18]

Ultrasonic sensors were placed on the specimen. With the help ultrasonic sensors Lamb waves were sensed to assess the health of a damaged joint (to assess the difference between a healthy joint and damaged joint). The signals before and after the damage for a given joints were compared to evaluate the location of the damage on the joint. The sensors were able to show the presence of damage in the joint. Delamination and hidden damage in the laminate was visualized as changes in the propagating Lamb wave characteristics [18].

In 2012, Weyrauch et al studied the joining of composite laminate for complex structures [19]. The main goal of the study was to reduce the bonding risks and use the bonding potentials of composite design. The study focused on adhesive bonding that provides a significant cost and weight savings using OOA infusion processes [19]. The challenge was to create an interaction between the preform infusion and the adhesive bonding processes [19]. The study was applied on a generic flap track. It consisted of 2 side panels, 2 upper panels and a lower panel. After manufacturing the flap tracks, the parts were tested to assess the strength of different bond-line thicknesses [19]. Also, an investigation of different surface treatments was carried out. The study showed that all surface treatments improved the wetting of the bonded surfaces compared to untreated specimens [19]. All methods for surface treatment delivered similar results. However, it is interesting to mention that grinding and grid blasting produced the lower scatter in the result. Moreover, it was shown in the study that there was a slight improvement of the shear strength when the web was misaligned in the preformed Pi. However, the misalignment is not recommended. Also, it is not recommended to grid blast all the surfaces especially in the preformed Pi-Joint due to the difficulty to reach both sides of the gap [19].

1.5. Motivation

Research is required to advance the technology of OOA to obtain a part with similar quality to autoclave process especially for complex components.

The focus of this research is to combine a low cost out-of-autoclave manufacturing process with an innovative joining Pi-Joint design to ultimately reduce the weight.

Most of the literature focuses on the challenges related to the OOA manufacturing of simple geometries or the mechanical performance of Pi-Joints. There has not been a research study that relates the manufacturing challenges of OOA to the mechanical performance of a Pi-Joint, making that gap in knowledge a prime topic of research. The combined effect of the geometrical parameters, such as the radius variation on the porosity level and compaction, and the adhesive bonding on the resulting mechanical performance of the Pi-Joint has yet to be investigated thoroughly.

1.6. Research Objectives and Thesis Organization

The objective of this thesis is to develop a better understanding of the manufacturing and mechanical performance of Pi-Joints made of OOA materials.

To achieve the desired objective, the following tasks were performed:

1. An experimental study on the variations of the manufacturing techniques for Pi-Joint is presented in Chapter 2.
2. A numerical model of the Pi-Joint is developed in Chapter 3 to understand its mechanical behaviour under a pullout load.
3. An experimental study of the first mode of failure of a Pi-Joint is carried out in Chapter 4 to substantiate the numerical approach.

Chapter 2.

Manufacturing of Secondary Bonded Pi-Joints

This chapter describes the experimental procedure to manufacture composite bonded Pi-Joint using the OOA process. Section 2.1 provides details on the materials used. Section 2.2 explains the laminates' design and layup. Section 2.3 describes the fabrication procedure of the Pi-Joint using the OOA process. Section 2.4 describes the bonding procedure of the web onto the preformed Pi. Section 2.5 explains the cutting and trimming of the Pi-Joint. Section 2.6 provides the physical measurement results of the manufactured samples.

2.1. Material

2.1.1. Prepreg Materials

The material used in this research consists of an epoxy resin pre-impregnated carbon fibre (prepregs). An unidirectional ply is used as filler at the radius of the Pi-Joint. The woven fabric used is an 8 Harness-Satin (8HS) as the fabric architecture is more pliable than a plain weave (PW). Therefore, it is easier to conform to a curved surface like the Pi-Joint radius region. Typical 8HS material is shown in Figure 10.

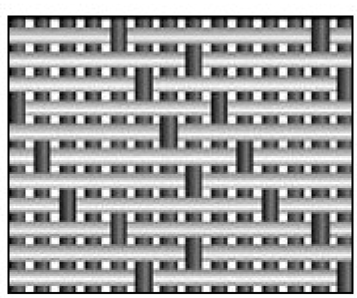

Figure 10 8HS Plies [21]

The prepreg system by Cytec Engineered Materials is a toughened epoxy resin prepreg system; the fibres are T40/800B and the resin system is 5320 Epoxy. As shown in Figure 11, there is a layer of dry fibre in the middle of the ply to create an air channel system to evacuated air during the debulking and curing process.

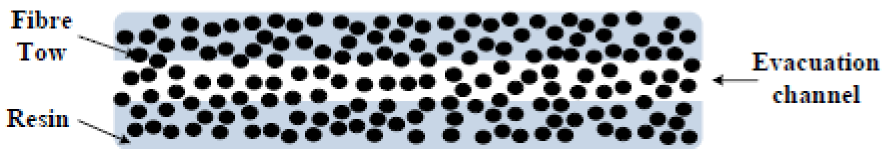

Figure 11 Prepreg CYCOM 5320 Epoxy Resin System [22]

2.1.2. Consumable Materials

Various consumable materials are required for bagging and curing during the OOA process. Most of these materials are made for one-time use and provide air network channels to evacuate air and volatiles while transferring the compaction pressure during the debulking and curing process. The table below shows the consumable materials that were used for this project:

Materials	Specifications	Purpose
Breather cloth	Airtech Ultraweave 606 Nylon breather	Create a network of the air channels for voids and volatiles to be evacuated from laminate by means of vacuum pump.
Perforated release film	Airtech A4000 Fluoropolymer	Prevent through-thickness resin bleed during cure. Provide non-sticking surface between the part and the breather. Provide and air path between the part and the breather.
Non-perforated release film	Airtech A4000 Fluoropolymer	Prevent through-thickness resin bleed and air flow during cure. Provide non-sticking surface between the part and the.
Vacuum bag	Airtech Wrightlon 7400 Nylon vacuum film	Seal the laminate and provide compaction pressure under atmospheric pressure.
Sealant tape	Airtech GS213 sealant tape	Seal the vacuum bag. Prevent in-plane resin bleed. Provide an edge breathing system.
Peel ply	Airtech peel ply	Provide a uniform rough surface free of any contamination for bonding.
Fibre glass	3 inch-wide plain weave fibreglass fabric	Provide a network to extract air and volatiles from the laminate to the breather cloth.

Table 1 Details of consumable materials

2.1.3. Tools

Three aluminum tools were used to manufacture the bonded Pi-Joint. The first tool was used to produce pressure intensifiers, see Figure 12. The pressure intensifier acted as a flexible tool used in the manufacturing of the Pi-joint.

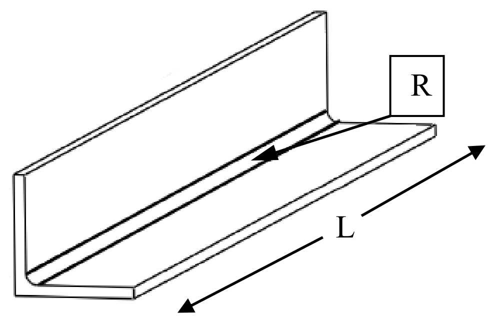

Figure 12 L-Shape tool for the manufacturing pressure intensifiers

The purpose of the L-Shape tool was to control the pressure intensifier radius, R=9.53 [mm]. The length of the tool, L, was 915 [mm].

The second tool was used to lay up the plies and cure the Pi-Joint. The essential dimensions of the tool are shown in Figure 13. The base-tool was a 12.7 [mm] thick aluminum plate. The insert-tool was held vertical on the base-tool with the help of four L-shape brackets. The brackets were adjustable in two directions along the base-tool to allow for adjustment. The insert-tool could be removed to allow accessibility for laying-up the laminate. The insert-tool was also adjustable in up and down direction to be able to control the tolerance and the geometry of the Pi-Joint.

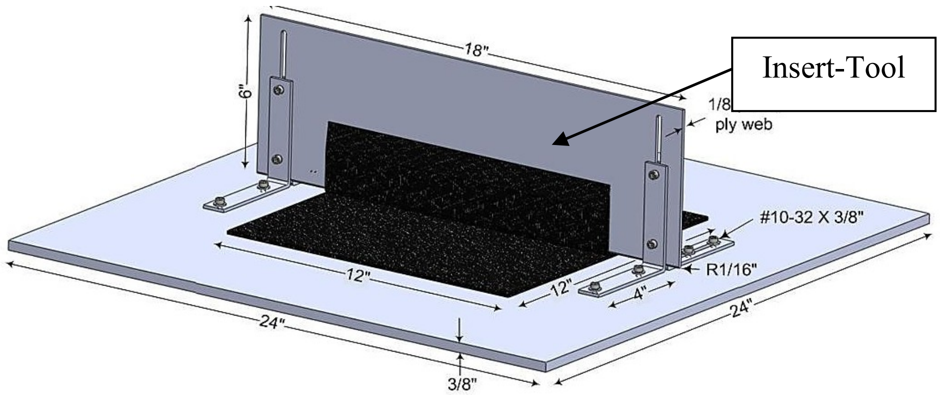

Figure 13 Principal lay-up tool for the manufacturing of Pi-Joint

The third tool was a flat plate used to lay-up the web. Figure 14 shows the dimensions of the flat plate.

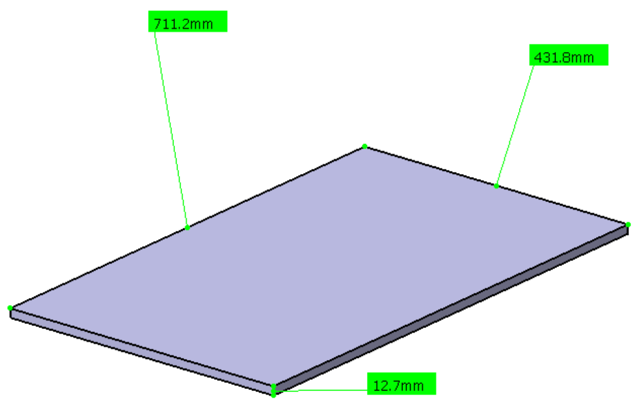

Figure 14 Tool used for manufacturing of Pi-Joint web

2.2. Pi-Joint Laminate Design

The following section explains the design that is show in Figure 15. A typical thin laminate for a non-pressurized skin section of a lightweight aircraft is about 2.5 [mm]. In this research study, the laminate representing the skin in the joint consists of eight plies of 8HS. The ply orientation of the skin is $[\pm45, 0/90, \pm45, 0/90]_s$. There are two plies that make a U-Section plies in the preformed Pi. The ply orientation of the U-Section is $[0/90, \pm45]_T$. The main purpose of these two plies is to reduce the peeling effect of the web. The L-Section laminate consists of four plies on each side, their purpose is to transfer the shear load from the web to the skin. The ply orientation for this section is $[\pm45, 0/90, \pm45, 0/90]_T$. To reinforce the skin, two plies are placed on the skin under the preformed Pi. The orientation of the laminate for the skin reinforcement is same as the U-Section section, $[0/90, \pm45]_T$. Since there is a substantial percentage of the load transferred through the radius of the L-Section laminate, it is important to control the outer radius of the laminate at the radius of the Pi section. This is not feasible for some manufacturing techniques because the outer radius of the laminate is on the bag side. It is noteworthy that as the radius is decreased the stress concentration at this part of the laminate is increased.

Statistical variability of the lamina, porosity and cutting quality of the joint affect the strength of Pi-Joint. It is important not to make the Pi-Joint too narrow that the test result would not high variation from one specimen to another specimen. Consequently, the width of the Pi-Joint is 50.8 [mm]. The expected unintentional manufacturing defect size would be in order of 1.0 to 3.0 [mm].

In case of any misalignment of the web position to the grips of a mechanical testing machine, it is important not to allow side load on the web which would reduce the strength of the joint. Therefore the height of the web has to be long enough to minimize any side-load transfer to the Pi-Joint from the mechanical testing machine grip. The designed height of the web is 203.2 [mm] to minimize the side load transfer of the grip by reducing the stiffness. The manufactured web height is 228.6 [mm], about 25.4 [mm] longer than the designed dimension to allow some space for trimming. Figure 15 is the lay-up drawing of assembled Pi-Joint.

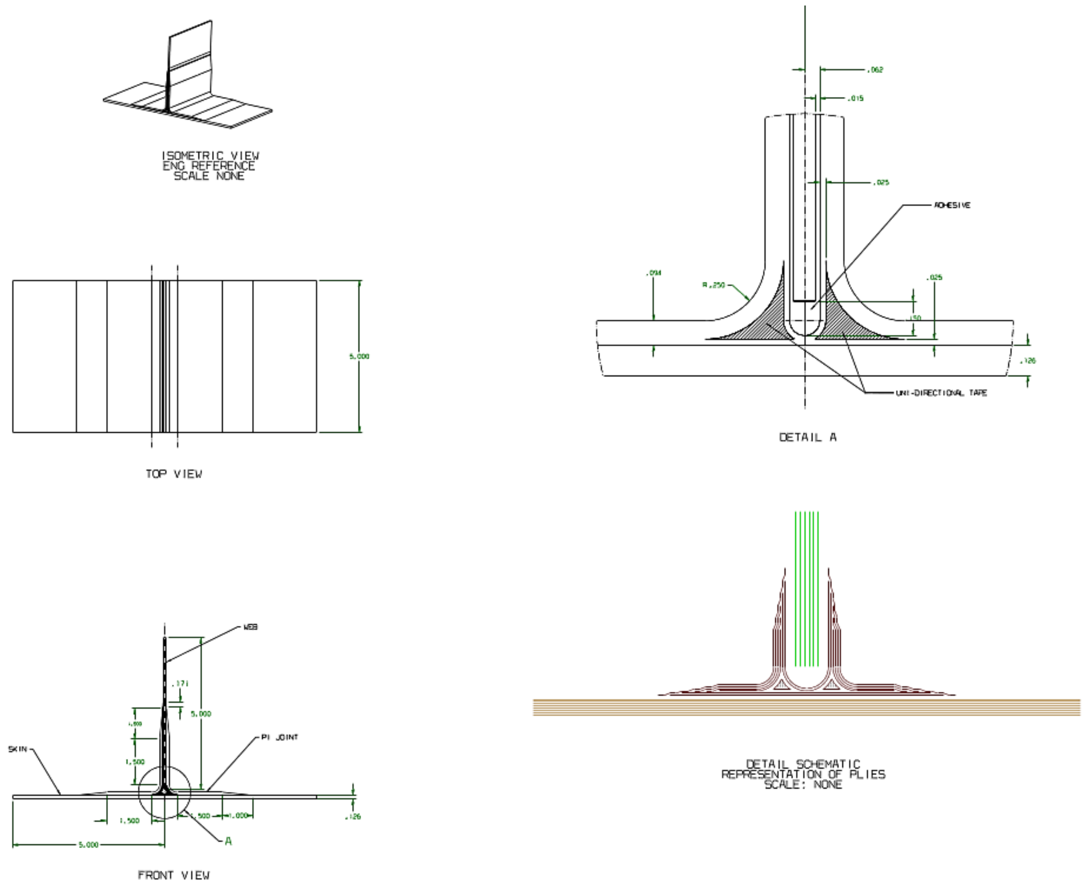

Figure 15 Lay-up drawing of the Pi-joint Unidirectional filler configuration

2.2.1. Adhesive Film

Since the skin is already pre-cured and the geometry of preformed Pi is stable, it is a challenging procedure to inset the adhesive film between the Pi and the web. The precured web must be inserted into at close tolerance of preformed Pi. To facilitate the placement of the adhesive, there is a designed gap of 0.5 [mm] between the web and the Pi. The adhesive film thickness is 0.40 [mm]. The adhesive film is wrapped around the bottom half of the web and inserted into the preformed Pi. There is a possibility of tearing the adhesive film and not being able to slide the adhesive all the way into the bottom of the Pi. To mitigate this risk, it is important to use an adhesive film that has a carrier mat such as FM 300-2M. Moreover, there is a light spring back of the preformed Pi that helps to insert the web with the adhesive film into the cavity of the preformed Pi. The width of the adhesive film is slightly larger than the space available in the preformed Pi to ensure that the entire bondline surface is covered by adhesive. A schematic view of adhesive film is shown in Figure 16.

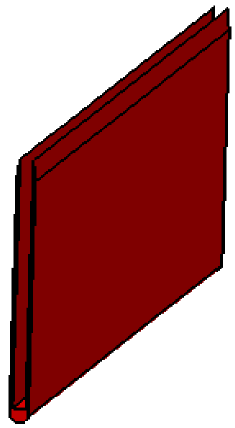

Figure 16 Schematic view of adhesive film

2.2.2. Web

The web is pre-cured separately from the preformed Pi-Joint. The web consists of eight plies with a $[\pm45, 0/90, \pm45, 0/90]_s$ lay-up orientation . The pre-cured web is 228.6 [mm] in height and 330.2 [mm] in width. A schematic view of the web is shown in Figure 17.

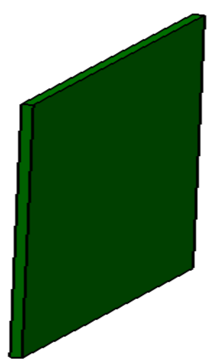

Figure 17 Web of Pi-joint

2.2.3. Preformed Pi-Joint Co-Cured to Skin

The preformed Pi-Joint, shown in Figure 18, is co-cured to the skin to ensure reliability of the load transfer throughout the service life of the part. The most challenging step is to manufacture the preformed Pi with the skin. At the radius of the preformed Pi, the plies must be bent to their limit to conform to a very small female tool, an almost zero radius contour. U-Shape plies act like a female tool for the L-Shape plies. The bag pressure is limited to atmospheric pressure. There the ply adjacent to the bag is atmospheric pressure. Since the tool, bag and laminate are in equilibrium; the compaction force is constant. As the layers are closer to the tool surface the compaction pressure drops below atmospheric pressure. To have a conformed Pi-Joint, uniform compaction and evacuation of the volatiles and air from the laminate is essential.

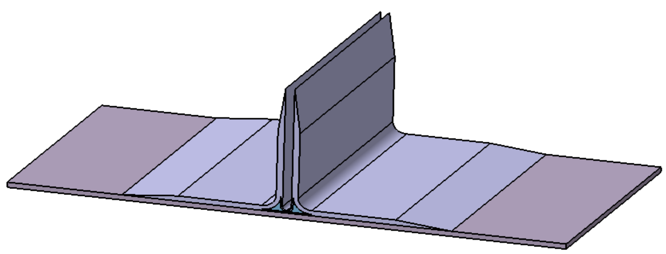

Figure 18 Preformed Pi-Joint co-cured to skin

2.2.4. Post Curing and Bonding of the Web to Preformed Pi

The cured Pi-Joint is 330.2 [mm] in width, 330.2 [mm] in length, and 232 [mm] in height. After the part is manufactured, it is cut to five 51 [mm] coupons in width. The complete Pi-Joint is shown in Figure 19.

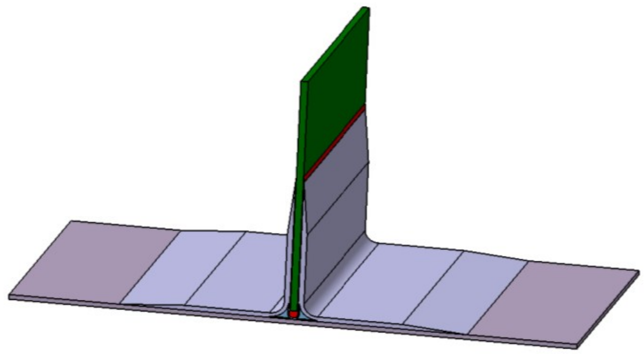

Figure 19 Post cured and bonded Pi-Joint

2.3. Pi-Joint Fabrication

Before fabricating the Pi-Joint, all manufacturing tools are polished to ensure the tool is free of any contamination or scratch marks that might be transferred onto the part. The tools are then cleaned with a cleaning agent such as Propanol/Acetone. The principal manufacturing tool shown in Figure 13 is surface treated with a release agent to prevent the cured part from sticking to the tool.

2.3.1. Web Fabrication

Surface preparation of the web is crucial to ensure the bondline is strong and free of any defects. Release agent is not used on the surface of the web tool because of the possibility that it would stay on the surface of the web and contaminate the bonding surface. First, a layer of non-perforated release film is placed on the aluminum tool and taped to the tool to prevent the release film from any movement during curing. The release film is cut 25 [mm] longer than the dimension of the web from four sides. A peel ply with similar dimensions to the release film is placed and taped on top of the release; the accuracy of dimensions of the peel ply and release film are not of importance. However, it is critical to ensure the laminate is 25 [mm] smaller than the peel ply and release film to prevent the laminate inform getting in contact with the tool or other consumables.

A thermocouple is placed half way the width of the web at the edge where the laminate layup would start. See Figure 20 for the location of thermocouples.

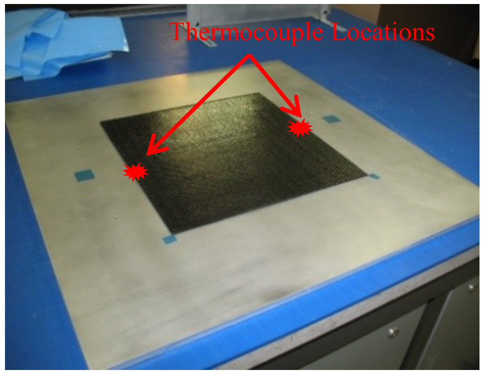

Figure 20 Location of thermocouples

The first ply is placed on the tool. After the placement of the second ply, the laminate is debulked for half an hour for every ply after that. The purpose of debulking is to lock the plies together and prevent them from any movement, as well as to extract air within the plies as much as possible. 8HS plies themselves are neither balanced nor symmetric. Therefore, during the layup an extra care is required to ensure that the laminate is symmetric, due to the weave pattern, to minimize any warping and residual stress in the laminate. After the last ply is placed, there is a second thermocouple placed on top of the laminate at the same location of the first thermocouple. Then another peel ply is laid down on the laminate. On top of the last peel ply, there is another layer of perforated release film laid down. A layer of breather was laid on the release film to create the air network channel in the laminate. The lower half of the vacuum valve was placed on the corner of the breather. After a layer of vacuum bag is placed on top of the layup and sealed with a sealant tape all around the tool. The laminate is left under vacuum for eight hours before curing to allow entrapped air to be evacuated before the start of the cure cycle.

2.3.2. Skin with the Preformed Pi Fabrication

The first step is to prepare the tool for the ply layup. The surface of the main tool and insert-tool are polished to ensure the tools are free of any surface marks, scratches or contamination, similar to the web tool. For convenience, the release agent is used on the main tool. However, a non-perforated release film is used on the insert-tool instead of a release agent (for reasons similar to the web tool preparation).

A thermocouple is placed under the laminate of the preformed Pi at root of the Pi-Joint on tool surface to monitor the temperatures of the laminate on the tool side to ensure the degree of cure, the oven and part temperatures are monitored during cure for each part at each curing step (pre-cure and post-cure).

The first and second plies are laid down on the main tool. The plies are debulked for half an hour. Then the third ply is laid down and debulked. These steps are continued until all the plies of the skin are laid down. See Figure 21 for the skin plies during layup.

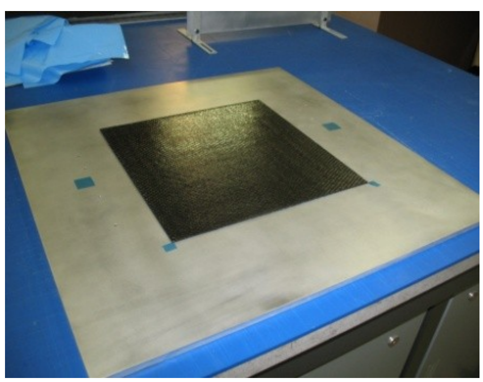

Figure 21 Skin plies layup

The second step is to lay down the skin reinforcement plies. The first ply of skin reinforcement is laid down followed by debulking. Then the second ply is laid down followed by debulking. See Figure 22 for the skin reinforcement plies during layup.

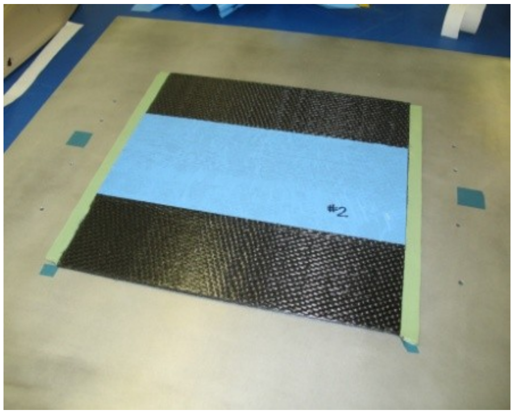

Figure 22 Skin reinforcement plies layup.

The third step is to lay down plies of U-Section over the insert-tool. First a layer of release film is wrapped around and taped to the insert-tool. Then a layer of peel ply is placed all around and taped to the insert-tool. Consequently, the first and the second plies of the U-Section are placed on the insert-tool. After laying the second ply, the insert-tool with the plies is placed and bolted onto the principal tool. Another debulk is done to remove the air between U-Section plies and lock the plies together. See Figure 23 for the U-Section plies Layup.

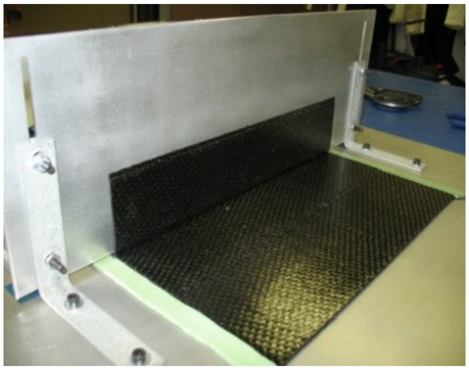

Figure 23 U-Section plies lay-up over the insert-tool

The last step of the layup is the most crucial; the quality of the laminate at the radius is dependent on the procedure used in this step. To study the effect of various layup procedures on the laminate quality at the radius, four different Pi-Joint configurations were used to layup the laminate at the radius. The different configurations are presented below:

1. The easiest and least costly technique is to layup the L-Section of the preformed Pi plies followed by debulking of each ply. It is important to ensure the first ply of L-Section is well squeezed into the radius of the preformed Pi to minimize any void or entrapped air in the cavity of the radius, see the red arrow in Figure 24. Therefore, before debulking the ply, each ply is pushed into the corner with a rounded edge metallic plate. The two arrows in Figure 24 show the corner where the plies are squeezed to maximized compaction. This configuration is referred as Baseline.

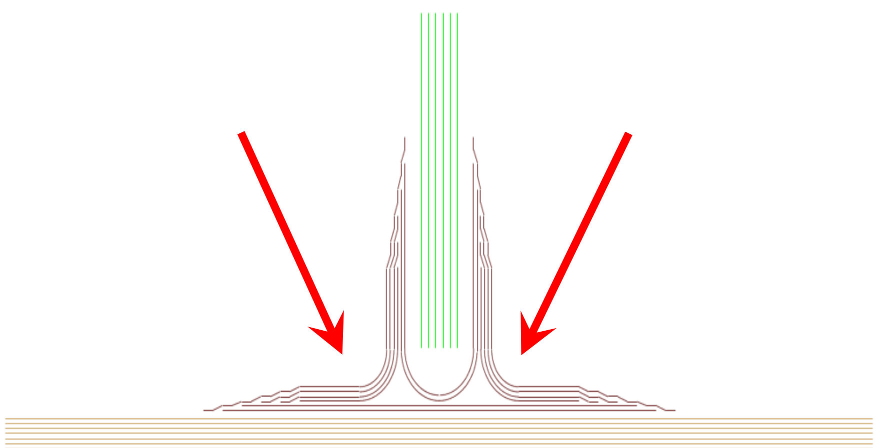

Figure 24 Schematic view of Baseline manufacturing technique

2. The second technique is to follow the first technique but after all the plies are laid down, a pressure intensifier that is made of rubberized silicon is placed over the plies at radius. The L-Section plies at the radius follow the shape of the pressure intensifier; therefore, the L-Section plies are well squeezed into the radius. See Figure 25 for the schematic view of the

pressure intensifier. This configuration is referred as Pressure Intensifier configuration.

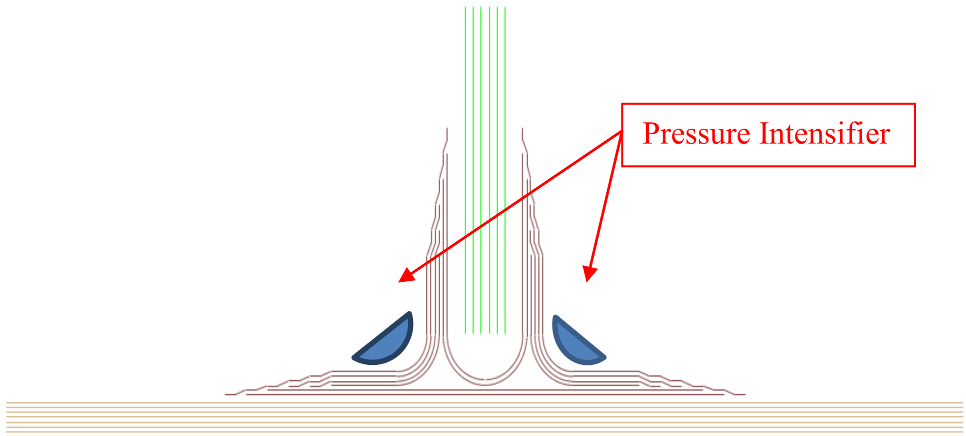

Figure 25 Schematic view of Pressure Intensifier manufacturing technique

3. The third technique is to overlap the plies at the radius. As the vacuum pressure is applied for compaction, the plies are pressed against the tool. If the plies are not able to slide over each other to conform to the geometry of tool or the plies at the lower level, the plies would bridge. To eliminate this phenomenon, the L-Section plies at the radius are cut and overlapped for at least 12.5 [mm]. In this case, the plies can slide over each other at the radius to reduce the bridging effect under the vacuum pressure. See Figure 26 for schematic view of the over plies at the radii. This configuration is referred as Overlap configuration.

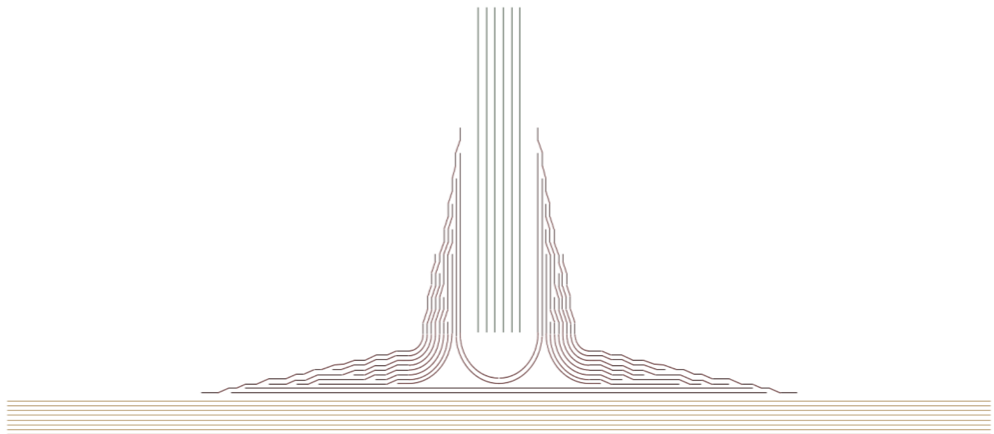

Figure 26 Schematic view of Overlap manufacturing technique

4. The fourth technique is to place a unidirectional ply insert at the radius to fill the void. The red arrow in Figure 27 shows the schematic presentation of the unidirectional ply at the radius. This configuration is referred as Unidirectional Filler.

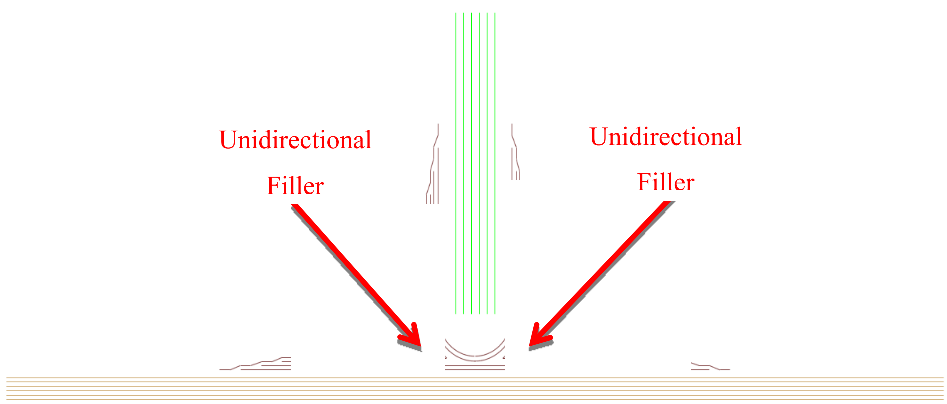

Figure 27 Schematic view of Unidirectional Filler manufacturing technique

A unidirectional ply of 19 [mm] width was rolled with hand and pressed as hard as possible with fingertips to minimize the rolling radius. Then the insert was placed at the radius and squeezed into the radius with a rounded edge metallic plate to compact the unidirectional insert as much as possible. Subsequently, the L-Section plies were laid up similar to the first manufacturing technique. Figure 28 shows the location, where the unidirectional plies were inserted.

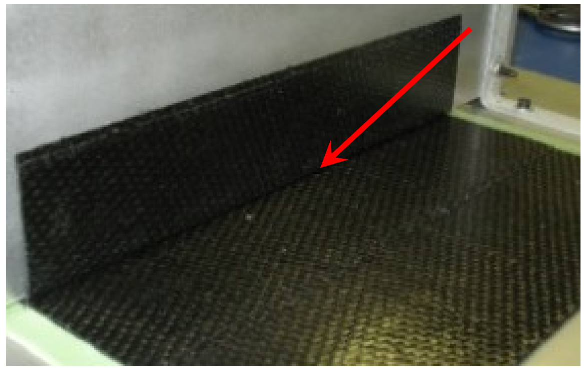

Figure 28 The location where unidirectional plies were inserted

After laying all the plies of the laminate, a network of air channel system, the edge breather, was incorporated to the edge of the laminate to allow the extraction of air and volatiles from the laminate during debulking and curing. This network is one the main features that distinguishes OOA from an autoclave cure process. The edge breather consists of dry woven fibreglass fabric wrapped around a sealant tape. The sealant tape and the fabric are placed along each edge of the laminate, as shown in Figure 29.

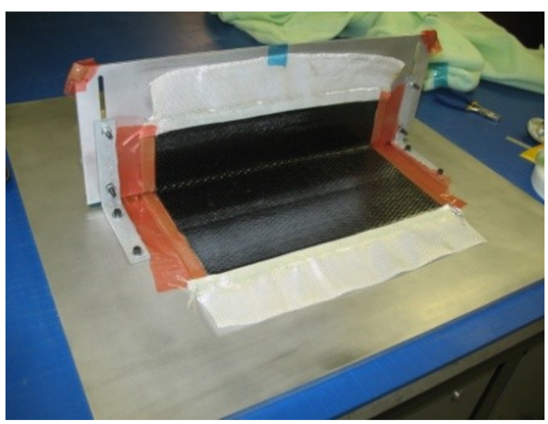

Figure 29 Edge breather set up

It is important to ensure that the fibreglass fabric is in contact with all the plies of the laminate stack as much as possible for an efficient air channel network. Since the fibreglass is dry, the vacuum is applied over the laminate and at the edge of the laminate through the edge breathing (fibreglass). The porpose of the sealant tape is to secure the fibreglass during handling, bagging and curing. Moreover, the sealant tapes build a dam for the resin to prevent resin bleed. The dam is essential for OOA process because the OOA prepreg is designed with net resin/fibre fraction.

The second to last step was to place another thermocouple on the laminate under the perforated release film. After all the plies are laid up on the laminate a thermocouple was placed on radius of the preformed Pi to measure the temperature gradient of the laminate at the radius.

The final step before curing was to bag the laminate and leave it under the vacuum for 8 hours. The laminate was covered with a perforated release film. Subsequently a layer of breather was positioned over the perforated release film. Sealant tape was placed at sharp corners of the tool to pervert the bag to be punctured. Two vacuum valves were placed on the tool beside where it was in contact with the breather beside the laminate. Vacuum bag was placed all over the tool and sealed by a sealant tape as shown in Figure 30. Finally vacuum pressure was applied through one vacuum connector for eight hours.

Figure 30 Final debulk of the laminate before placing in oven

The laminates are cured in a temperature-regulated oven where temperature is measured and controlled. The oven automatically controls the heating power to ensure the target temperatures of the oven during the curing process are of desired setting.

The cure cycle consisted of four phases:

1. A debulk at room temperature to extract entrapped air before impregnation of the fibres when resin viscosity drops.
2. The first temperature ramp to heat the tool and the laminate to the desired temperature. The ramp up rate is 1.67°C/minute. Moreover, the viscosity of the resin drops slowly as the temperature is increased. Consequently, fibre filaments are impregnated within the fibre tows.
3. Dwell at a temperature that allows cross-linking of polymers. The resin viscosity increases as polymers cross-link. The first dwell temperature is 92°C. The dwell time is 8 hours.
4. Ramp down of the temperature so the parts cool down to room temperature. The ramp down rate is 1.67°C/minute to the room temperature.

The debulk time, ramp rates, dwell temperatures and dwell times were selected based on the material supplier recommendations. Usually these recommendations are based on prepreg system for efficient air removal during debulk and complete impregnation of fibres before resin cure.

The cured performed Pi is shown in Figure 31 after the laminate was taken out of the tools and it is ready to be bonded to the web.

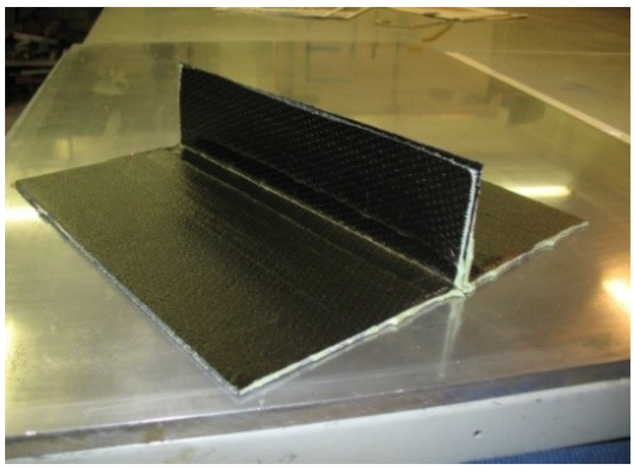

Figure 31 Cured Preformed Pi-Joint with Skin

2.4. Bonding the Web into the Preformed Pi

The peel ply was carefully removed from the preformed Pi. The second step was to remove the peel ply from the web and to place the adhesive film over the web. It is important not to touch the bonding surface with any object due to possible surface contaminations. Then the adhesive film was folded into half. Next the adhesive film was applied to the lower half of the web. A thermocouple was placed between the adhesive film and the web at one edge of the joint so the temperature of the bond-line was measured during post cure. It is important to note that after peeling the peel ply from the web, the surface of the web is still chemically active and ready to be bonded. The contamination of the surface of the bond-line can reduce the ultimate strength of the secondary bond.

Subsequently, the web is inserted into the preformed Pi. The edges of the U-Section in the preformed Pi are very sharp. During inserting the web into the Pi cavity, it was very important not to push the web against the edges of the Pi because the adhesive film might break. Removing the adhesive film and reapplying the over the web might contaminate the bond-line surfaces. It is important to make sure the web was pushed all the way to the bottom of the cavity.

The Pi-Joint now was placed over the main tool and a layer of perforated release film was applied over the joint. A layer of breather was placed over the perforated release film. The Pi-Joint was bagged with a vacuum valve inside the bag. The Pi-Joint was placed into the oven for the post-cure of the laminate and curing the adhesive. The cure cycle used to post-cure the laminate was as such:

1. Debulking at room temperature to extract entrapped air before the adhesive viscosity drops.
2. The first ramp up of the temperature to heat the tool, laminate, and adhesive film to the 120°C. The ramp up rate is 1.67°C/minute.
3. Dwell to a temperature that allows the adhesive viscosity to drop and to wet the bond-line and fill up and small surface roughness due the peel ply. At this step the adhesive starts cross-linking and cures slowly. At the same time more crosslinking happens in the laminate and the degree of cure is going higher and the higher. The dwell time is 4 hours.
4. Ramp down of the temperature so the parts cool down to room temperature. The ramp down rate is 1.67°C/minute to the room temperature.

After the part was taken out of oven, all the consumables were removed and the part was ready to be cut to the desired dimensions.

2.5. Cutting and trimming the Pi-Joint

It is very important to have a smooth quality edge cut, especially at the root of the Pi-Joint. Any noticeable edge roughness would reflect into reduction of mechanical strength due to the stress concentration and possible delamination. The Pi-Joints were cut at the Institute for Aerospace Research, National Research Council Canada.

Since the Pi-Joints were not flat, they were not easy to be cut with a table saw. Moreover, any other type of cutting tool such as hand held tool does not guarantee the repeatable dimensions and quality of the cut. To overcome these challenges, the Pi-Joints were cut with a two-step operation:

1. The first step was to cut the skin and the root of the Pi-Joint with a table saw. See Figure 32 for the dimensions of the cut. The intension of this cut was to create smooth cut at the root of the Pi-Joint.

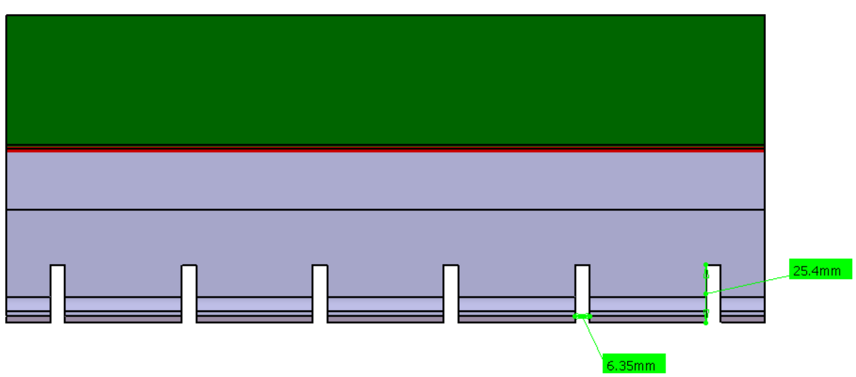

Figure 32 First step, Pi-joint cut

2. The second step was to cut the remaining section of the perform Pi and the web. A band saw was used to cut the remaining section and separate the

Pi-Joints from each other. See Figure 33 for a schematic cutting pattern. The width of the band saw cut was about three quarter of the table saw cut. The band saw cut dids not leave a smooth cut but since the weakest section of the joint is at the root and the band saw cut did not touch the root of the Pi-Joint, the band saw cut did not reduce the overall strength of the joint.

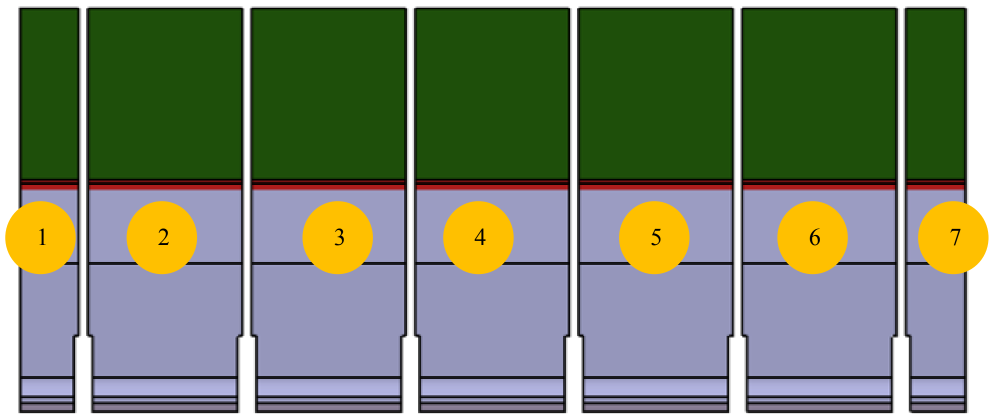

Figure 33 Second Step, Pi-Joint Cut

As it is depicted in Figure 33, the manufactured Pi-Joint was cut into 7 narrower Pi-Joint. The two ends Pi-Joint (one and seven) at the extremities were used for image analysis. Two, three, five, and six were mechanically tested. Four was kept and a reference to be used for post-testing results.

2.6. Pi-Joint Measurements

2.6.1. Sizes and dimensions of Pi-Joint

After the joints were cut into desired dimensions, the joints were measured. Although all the joins were meant to have the same dimensions because of cutting tolerance and slight different variations in the manufacturing techniques of the L-

Section radii, indeed, the different joints had slightly different dimensions. The dimensions of the joints are shown in the following table:

	Specimen Number (As in Figure 33)	W1 [mm]	W2 [mm]	W3 [mm]	T1 [mm]	T2 [mm]	R1 [mm]	R2 [mm]
Overlap	2	51.1	51.2	51.1	6.6	6.4	13.5	13.5
	3	51.2	50.7	51.0	6.5	6.4	13.5	13.5
	4	51.0	50.9	51.1	6.6	6.7	13.5	13.5
	5	51.1	51.0	51.0	6.5	6.6	13.5	13.5
	6	51.1	51.1	51.2	6.4	6.5	13.5	13.5
Base-Line	2	51.2	51.1	51.2	4.9	5.2	9.1	9.1
	3	51.2	51.2	51.3	5.0	5.2	9.1	9.1
	4	51.3	51.2	51.2	5.0	5.0	9.1	9.1
	5	51.2	51.1	51.3	5.2	5.2	9.1	9.1
	6	51.1	51.1	51.2	5.2	5.1	9.1	9.1
Unidirectional Filler	2	50.3	50.3	50.4	4.9	5.0	17.5	17.5
	3	50.3	50.3	50.3	4.9	4.9	17.5	17.5
	4	50.3	50.3	50.3	4.9	4.9	17.5	17.5
	5	50.9	50.8	50.7	5.0	4.9	17.5	17.5
	6	50.9	50.8	50.8	4.9	4.9	17.5	17.5
Pressure Intensifier	2	51.1	50.9	51.1	5.0	4.9	9.1	9.1
	3	51.1	51.0	51.1	5.0	5.0	9.1	9.1
	4	50.9	50.9	50.9	4.9	4.9	9.1	9.1
	5	50.8	50.8	51.0	5.0	4.9	9.1	9.1
	6	51.1	51.0	50.9	5.0	4.9	9.1	9.1
Pressure Intensifier (One Side Web Bonded)	2	51.0	51.0	50.9	5.0	5.0	9.1	9.1
	3	50.9	50.9	51.0	5.0	4.9	9.1	9.1
	4	51.1	51.1	51.1	5.0	5.0	9.1	9.1
	5	51.0	51.0	51.2	5.0	4.9	9.1	9.1
	6	51.0	51.0	51.0	5.0	5.0	9.1	9.1
Unidirectional Filler (One Side Web Bonded)	2	51.1	51.0	51.1	5.0	5.0	15.1	4.8
	3	50.9	50.9	50.9	5.0	5.0	15.1	4.8
	4	50.8	50.9	51.0	5.0	5.0	15.1	4.8
	5	51.1	51.0	51.1	5.0	5.0	15.1	4.8
	6	51.0	51.0	51.0	4.9	5.0	15.1	4.8

Table 2 Pi-Joints Dimensions

The nomenclature of the titles in the column of Table 2 is explained in Figure 34.

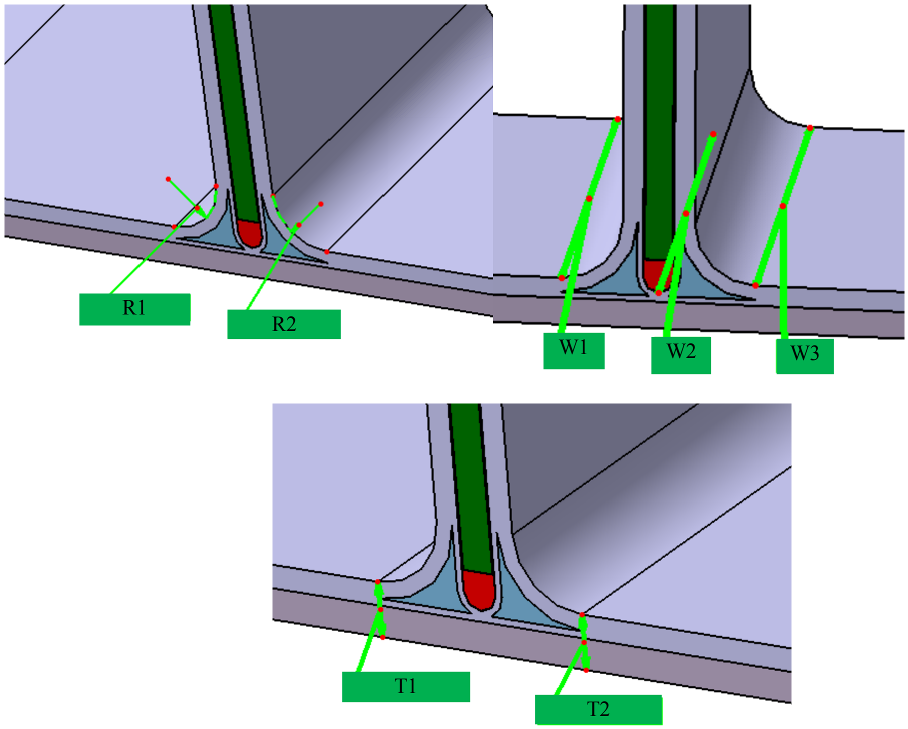

Figure 34 Nomenclature for Table 2

2.6.2. Porosity in Pi-Joints

Porosity was another important measurement that defines the performance of the part. The porosity was measured for four different zones as shown in Figure 35. It is expected to have a different porosity in the radii of the Pi-Joint.

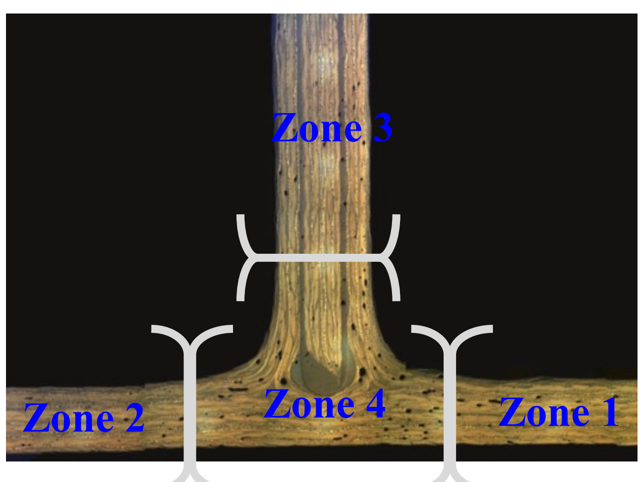

Figure 35 Different Porosity Measurement Zones

After the specimens were polished and analyzed under the microscope, two types of voids were observed. The first type was caused by lack of adhesive. One way to improve this void is to bond the web to the preformed Pi with more adhesive film. It was observed in the test that this type of void did not affect the overall strength of the Pi-Joint. The void in the adhesive was clearly seen at the root of Pi-Joint, as it is seen in Figure 36 b) and d). The other type of void seen in the specimens was porosity in the laminate. This particular void is of interest in this study. To be able to control porosity in the laminate, a great understanding of the material, process and the features in the part is required.

The Baseline configuration had the lowest porosity level in Zone 4, as it is shown in Figure 36 a). The second lowest porosity was observed for the Pressure Intensifier configuration in Zone 4. The Overlap configuration had considerably high porosity, 4.6% as it is tabulated in Table 3, in Zone 4. The other zones had acceptable porosity, below 3.0%. The worst level of porosity was observed for the Unidirectional filler configuration, as it is shown in Figure 36 d). Zone 4 had 7.4% porosity as tabulated in Table 3.

When the unidirectional filler was placed at the radii during manufacturing, the unidirectional plies were rolled and squeezed to reduce the void in the laminate. Since the unidirectional plies were not compacted, there was a large bulk factor in the filler. After placing the unidirectional filler at the radii, the L-Section plies were placed over the unidirectional filler. During the cure, the vacuum bag pressed the L-Section plies and locked the plies to the U-Section and skin plies. At the same time, the vacuum bag was trying to compact the unidirectional filler. Since the L-Section plies cannot get stretched, the unidirectional filler did not get compacted and the pressure applied on the unidirectional filler was not sufficient to collapse the voids.

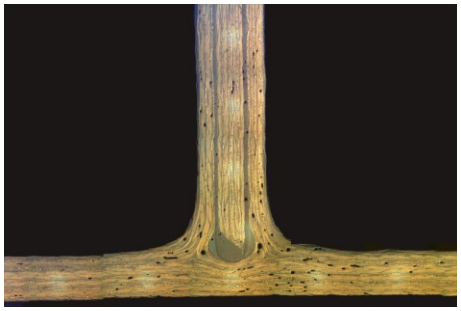

Baseline Configuration a)

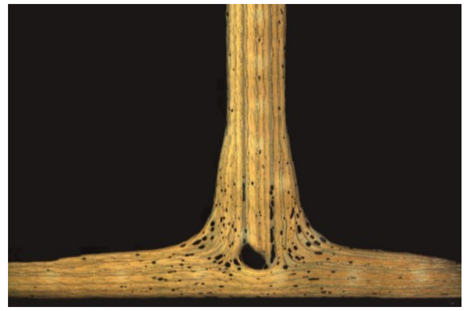

Overlap Configuration b)

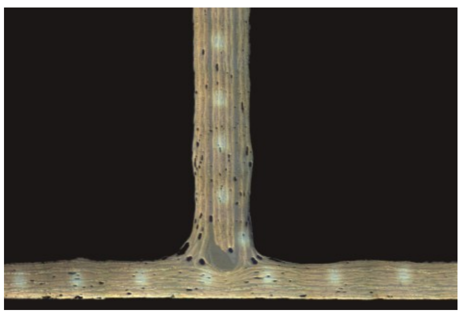

Pressure Intensifier Configuration c)

Unidirectional Filler Configuration d)

Figure 36 Cross section Cut of Polished Pi-Joints

	Configurations	**Base-Line**	**Pressure Intensifier**	**Over-Lap**	**Unidirectional Filler**
Percentage of Porosity	Zone 1	1.0%	1.0%	1.1%	1.0%
	Zone 2	0.5%	2.4%	0.7%	0.7%
	Zone 3	0.8%	1.9%	0.9%	1.4%
	Zone 4	2.8%	4.2%	4.6%	7.4%

Table 3 Porosity Measurement of the Zones in the Pi-Joint Configurations

2.6.3. Change in thickness at Radius in Pi-Joints

Another measurement that is important for Pi-Joint is the change in ply thickness at corner. Change in ply thickness at the corner showed two issues. The first one is how well the ply is compacted. The second is the amount of voids in the laminate compared to flat section. Higher thickness increase at the corner compared to flat section translates to less compaction and higher level of porosity at the corner. Of course this is not desirable.

The average of thickness between horizontal segment and vertical segment of L-Section plies were taken. Table 4 tabulates the the percentage increase of corner thickness compared to average thickness of L-Section.

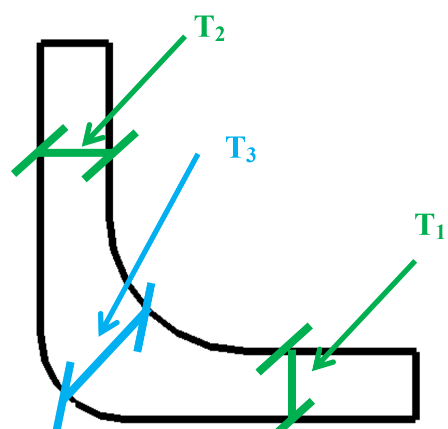

Figure 37 Nomenclature for Equation 1

Equation 1 $$\left(\frac{T_3}{\frac{T_1+T_2}{2}} - 1\right)\times 100 = Thickness\_Percentage\_Increase$$

The percentage increase for the Baseline is the lowest among all configurations except for Unidirectional filler configuration.

	Compare to	Base-Line	Pressure Intensifier	Over-Lap	Unidirectional Filler
Thickness Percentage Increase	Web	89%	110%	114%	36%
	Skin	85%	110%	109%	35%

Table 4 Ply thickness percentage increase at the corner

It is observed in Table 4 that Unidirectional filler configuration has the lowest thickness change at the corner. Ironically the corner in Unidirectional filler configuration has high level of porosity and it is not well compacted. It is because the L-Section plies are placed over the filler ply that is drenched with air (soft base). During the vacuum as the pressure was applied at the corner the vertical and horizontal segment of L-Section plies were locked and the atmosphere pressure was not able to press the corner to compact the filler.

Chapter 3.

Numerical Simulation and Analysis

Due to the complexity of the Pi-Joint geometry and the composite material orthotropic behaviour, it is not possible to obtain an analytical solution of the Pi-Joint mechanical behaviour. Therefore, finite element modelling is a practical technique to study the behaviour of the Pi-Joint. Of course, the estimation of the behaviour of the Pi-Joint coupons like the strength or the deflection is as accurate as the idealization process used. In this chapter the procedure to model the Pi-Joint and estimate the onset of the strength of the joint is described.

3.1. FEM Model

The joint is modelled with a commercial finite element modelling software. The pre-processor and post-processor is MSC PATRAN. The solver is MSC NASTRAN 2008. The solution used to estimate the strength and the deflection of the joint is SOL101. SOL101 is a linear elastic solution. Later on, non-linear static analysis, SOL106, is run only to validate the non-linearity behaviour of the joint. The result of the non-linear static analysis is not presented here. Non-linear static analysis is only used to demonstrate that the joint has a linear behaviour under the load condition applied to the models.

3.1.1. Creating the Geometry

The geometry of the Pi-Joint is modelled into a Computer Aided Design, CAD software and then it is imported into MSC PATRAN to be meshed. The Pi-Joint is modelled with five different surfaces (cross section surfaces):

1. Skin
2. Preformed-Pi
3. Unidirectional filler / Resin
4. Adhesive
5. Web

See Figure 38 for the surfaces used to mesh Pi-Joint.

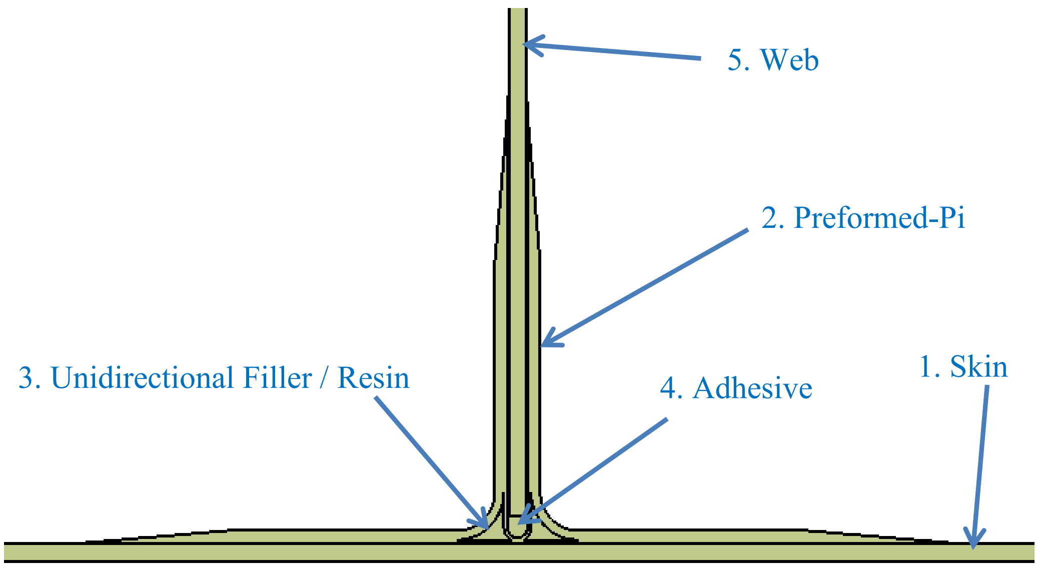

Figure 38 Surfaces used to mesh the Pi-Joint

3.1.2. Creating the Mesh

After importing the IGS model into MSC PATRAN, the surfaces were meshed with some ISO quadrilateral construction elements like CQuad4. Unidirectional filler surface was meshed using a Paver Mesh. The Paver mesh is an automated surface meshing technique that can be used with any arbitrary surface region. Paver meshing technique creates a mesh by first subdividing the surface boundaries into mesh points. Then mesher operates on these boundaries to construct interior elements.

The mesh seed for each curve was chosen so that each ply was represented by one element through the thickness of the laminate. After all the surfaces were meshed, the model was equivalenced. The thickness of the elements was 0.2 [mm]. To minimize the number of degree of freedom in the model and to ensure accuracy of the result, the element size varied in the model. The element width closer to the boundary conditions was 1.35 [mm]. The element width closer to the root of the Pi-Joint was 0.40 [mm]. The normal of the all elements were pointing toward aft-direction. Subsequently, the shell elements were extruded to create solid elements, CHEXA. There were 24 elements in the depth representing 50.8 [mm] width of the Pi-Joint coupon. Although the aspect ratio of the elements was slightly greater than the recommended ratio, the applied load and deformation of the element was not in the extruded direction. Therefore, the high aspect ratio of the elements did not affect the quality of the element and the accuracy of the results. See Figure 39 for the mesh of Pi-Joint.

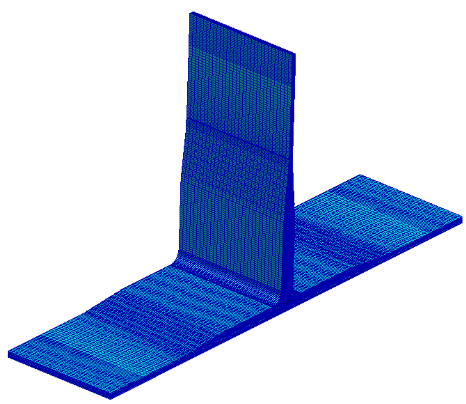

Figure 39 Pi-Joint mesh

The sample grid card is shown in Figure 40.

```
$1______2-------3_______4-------5_______6-------7_______8-------9_______
GRID    1               0.      .04710012.8
```

Figure 40 Sample grid card

The sample element card is shown in Figure 41.

```
$1______2-------3_______4-------5_______6-------7_______8-------9_______
CHEXA   1       1       844     837     743     742     3826    3825
        3731    3730
```

Figure 41 Sample element card

3.1.2.1.1. Mesh Properties

There are two isotropic material cards, MAT1 cards, created to represent:

1. Adhesive.
2. Resin rich area.

There are five other material cards created, MAT9 cards, to represent:

1. 8HS plies in cartesian coordinate system.
2. 8HS plies in cylindrical coordinate system.
3. 8HS plies in cartesian coordinate system 45° rotated**.
4. 8HS plies in cylindrical coordinate system 45° rotated**.
5. Unidirectional ply in cartesian coordinate.

** At the radius of the L-Section plies, a cylindrical coordinate was used to model the ply orientation. Since using the cylindrical coordinate system for plies with 45° orientation did not conform to the ply orientation of the joint. To overcome this lamination, an imaginary ply with a rotated 45° stiffness was modelled to represent 45° plies.

After creating the mesh for the Baseline, the L-Section radius was changed to match the manufactured radii, see Table 2 for the joints measurements. As the stiffness changes considerably at the radius (for Overlap and Unidirectional configuration, indeed, the stiffness of the joint at the radius was considerable greater than the Baseline) and stress concentration highly depends on the radius, it was important to idealize the joint as presentably as possible. See Figure 42 for the schematic view of the Overlap configuration mesh.

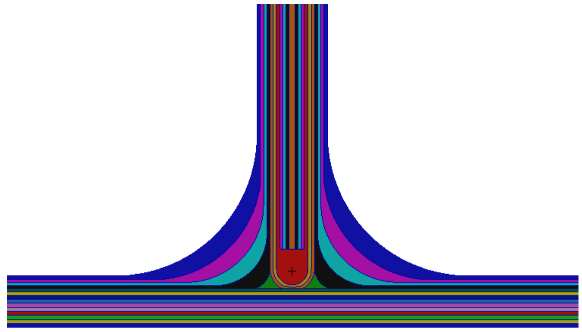

Figure 42 Overlap configuration mesh at the root of the Pi-Joint

(each color represents a ply in the Pi-Joint)

See Figure 43 for the schematic view of the Unidirectional configuration mesh.

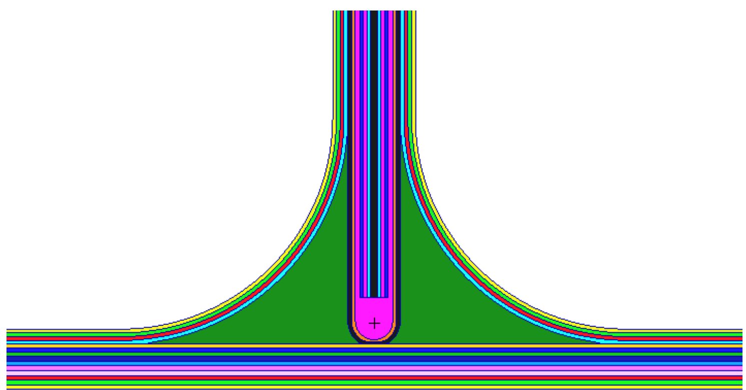

Figure 43 Unidirectional configuration mesh at the root of the Pi-Joint

(each color represents a ply in the Pi-Joint)

It is a general practice in composite to drop off the plies where there is no need for extra stiffness or strength. The drop off is done usually inside the laminate, ascending order, so the last ply that is exposed to the environment is covering the entire drop off plies. It is important to mention that such drop off is not practical to be modelled in FEM. Modelling ply drop off imposes so many constrains on the mesh, due the size and thickness of the drop off. Modelling ramp down of the drop off does not affect the stiffness of the global model. Moreover, there was no drop off in the critical section of the Pi-Joint. The drop off in the model is depicted in Figure 44.

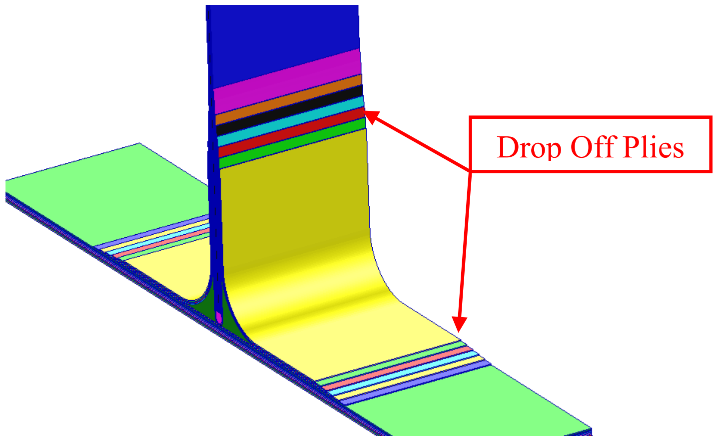

Figure 44 Idealized drop off in the FEM

After creating the material cards and the mesh, the properties of elements (PSOLIDs) were defined based on the material, geometry and ply orientations.

3.1.3. Loads/ Boundary Conditions

The test boundary conditions are shown in Figure 45. There are two boundary conditions applied on the model:

1. Displacement
2. Pull-Off load.

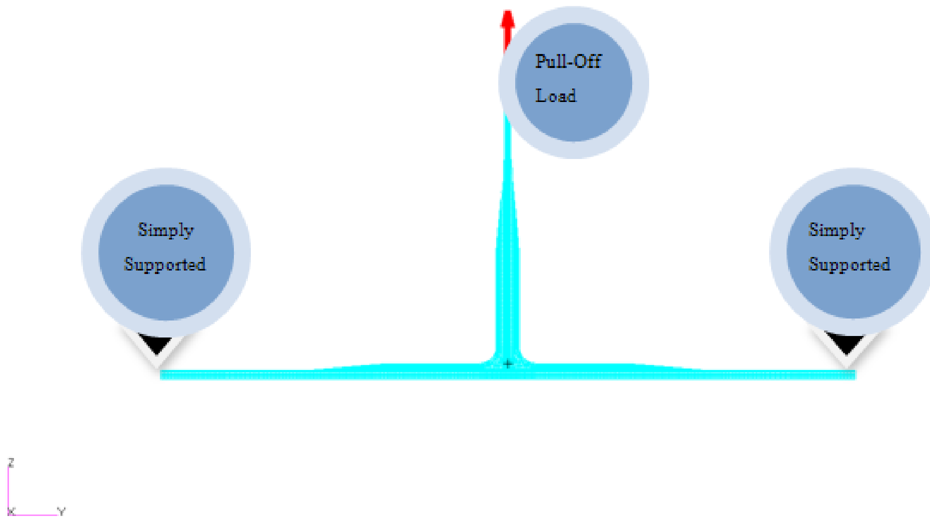

Figure 45 Boundary conditions of the test specimen

The boundary condition on the skin upper lamina was displacement, which was fixed in Z-direction at the extremities in the test. Due to the nature of numerical analysis, the model must be constrained in Y-direction and X-direction. Therefore, only grids on the top of the laminate on the right hand side of the skin, at the extremity, were fixed in 123-direction. The location of applied displacement boundary condition in the right hand side of skin is depicted in Figure 46.

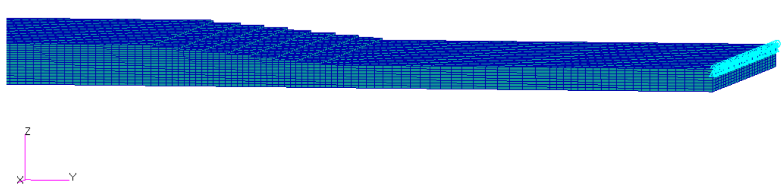

Figure 46 Applied boundary condition on the right hand side of the skin

The left hand side of the skin, at the extremity, was fixed only in the 13-direction. The location of the applied displacement boundary condition in the left hand side on the skin is depicted in Figure 47.

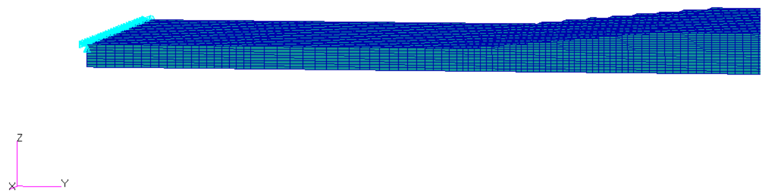

Figure 47 Applied boundary condition on the left hand side of the skin

The applied load in the test was a displacement rate that was translated into a pull-off force on the web. In the FEM model, the applied load on the web was simulated as pressure. The value was 6 894.8 [kPa]. The cross sectional area of the web was 121.55 [mm^2]. The total force applied on the web was 838 [N]. At this point the failure strength of the joint was unknown. Moreover the behaviour of the model is linear. Therefore, the applied load at this point (the first iteration) was an arbitrary value. After the analysis is run, the internal lamina stress in different directions, (σ_{xx}, σ_{yy}, σ_{zz}, and τ_{xz}) were compared to the lamina strength. Then the ratio of the lamina strength over applied load (838 [N]) was applied to applied load. The lowest force was the strength of the Pi-Joint. All the strength results presented in Chapter 3 are normalized.

The boundary condition on the web and the direction of the load is depicted in Figure 48.

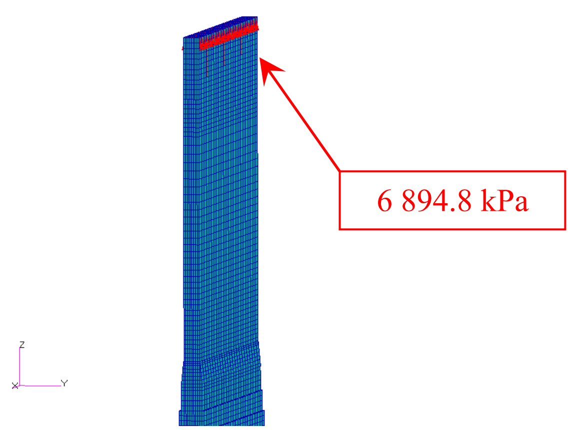

Figure 48 Applied boundary condition on the web

3.2. FEM Validation

To ensure that the models were free of any errors, the following checks were performed:

1. Epsilon*** smaller than $1x10^{-7}$.
2. Summation of single point constrains was equal to the applied loads (equilibrium condition).
3. No duplicated elements.
4. No crack in the model (equivalenced).
5. Element reliability threshold (geometry of the each element).
6. Material orientation.
7. Boundary conditions.
8. Maximum matrix to factor diagonal ratio smaller than $1x10^{7}$.
9. Maximum displacement should be in acceptable range (depending on the size and the behaviour of the model).
10. There is no free grid in the model.
11. All elements are with corresponding properties.
12. The behaviour of the model is as expected.

*** Epsilon is a measure of numerical accuracy and round off error provided in results files. This round off error is based on a strain energy error ratio.

After all checks were performed, the results were extracted from the model and compared to the material strengths as shown in the following section.

3.3. The FEM Results and Calculated Failure Strength

This section is divided into six different subsections and the results of the FEM are shown for each configuration. All the results shown here are normalized to the Baseline configurations.

3.3.1. Displacement

In this section the FEM displacement results for each configuration are explained. The displacement in the models was normalized by the maximum displacement of the Baseline configuration. The exaggerated displacement of the models is shown in Figure 49. Under the pull out load, the colour distribution from white to orange is fringed on the skin. At the root of the Pi-Joint and at the web, the colour plot was red because the root of the Pi-Joint was very stiff. It had the same displacement as the web. As per Figure 49, all configurations had a very similar behaviour.

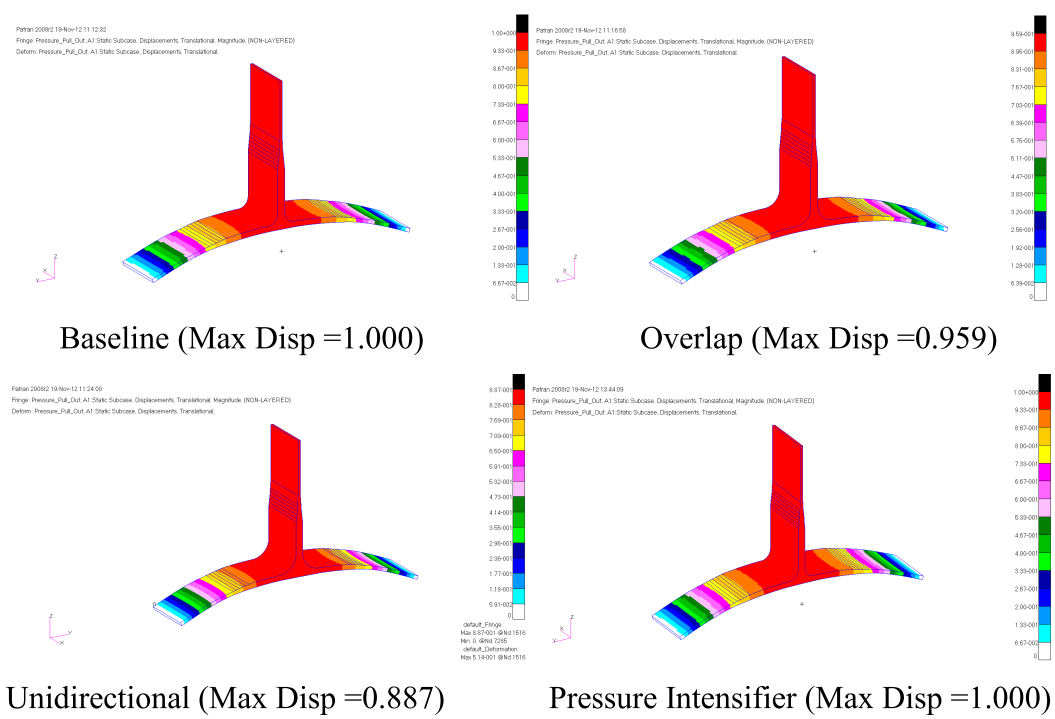

Figure 49 Normalized displacement plot

At the root of the Pi-Joint, the skin laminate did not bend considerably compared to the rest of the skin laminate. This means that the root of the Pi-Joint was not acting as a hinge-line. Moreover, it can be concluded that the load that was transferred from the web to the skin was not concentrated directly under the web at the root of the Pi-Joint. The load was distributed over a larger area, which reduced the stress concentration. Potentially the laminate at the radii of the Preformed Pi has a considerable contribution to the load transfer. By comparing the deformation for all the configurations, the stiffest joint in out of plane direction was to be Unidirectional followed by the Overlap configuration. Of course, the only manufacturing variation that was considered in the FEM was the change in the radius of the L-Section laminate. It can be concluded from the FEM result that as the radius gets larger, the out of plane stiffness of the joint is increased. The stiffness increased by 12% by increasing the radius by 92%. Indeed, increasing the radius was not an efficient way of increasing the stiffness of the joint. Nonetheless increasing the radius had a direct effect on the stiffness.

3.3.2. Adhesive

The bond-line failure is expected to happen under tensile stresses (Maximum Principal) in the adhesive or shear stresses at the bond-line (Maximum Shear). The maximum principal stress was located under the bottom of the web at the middle (through the depth) of the joint. The stress in the adhesive except at the root of the bond-line was less than 20% of the maximum principal stress in the bond-line.

As it is shown in the formula below, the high shear load can be transferred either by high shear stress or high surface area.

$$F_{shear} = \tau \times A_{shear}$$

In the case of Pi-Joint, there is a considerable load transfer from the web to the preform Pi through the bond-line because of the larger shear surface area not high shear stress magnitude. The highest loaded adhesive was for the Baseline and the Pressure Intensifier configurations and the lowest loaded adhesive was for the Overlap configuration as shown in Figure 50.

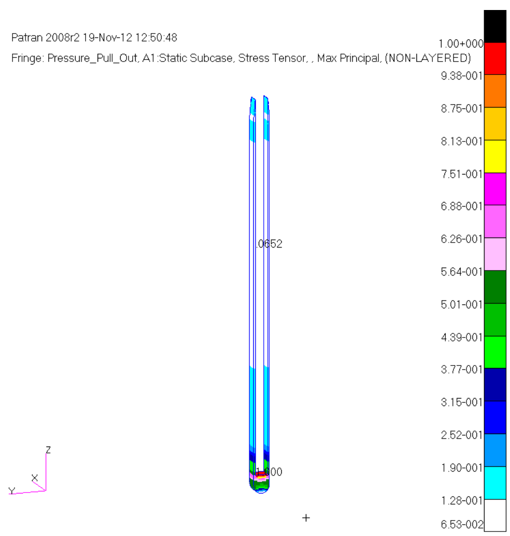

Baseline (Max Princ =1.000)

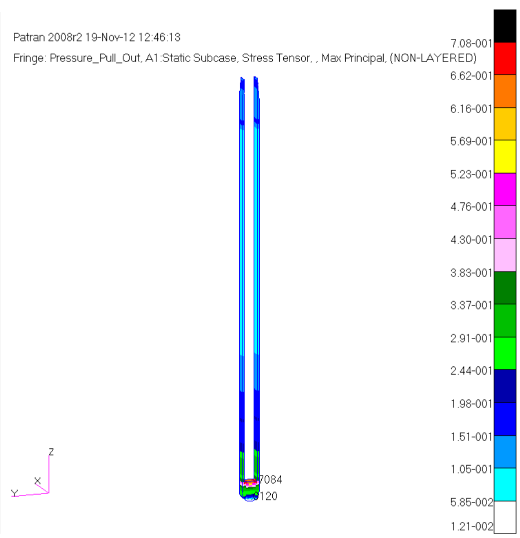

Overlap (Max Princ =0.708)

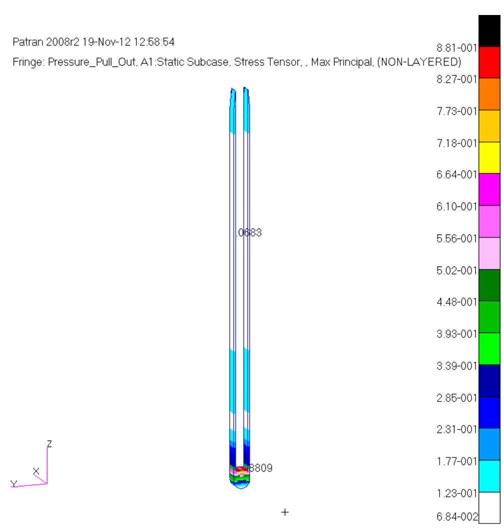

Unidirectional (Max Princ =0.881)

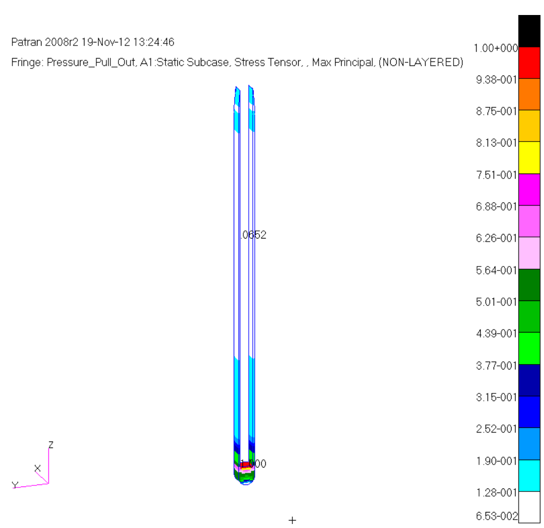

Pressure Intensifier (Max Princ =1.000)

Figure 50 Normalized Maximum Principal stress in the adhesive

Similarly the Maximum Shear stress in model was located under the root of the web at the middle (through the thickness) of the joint. The stress in the adhesive except at the root of the bond-line was less than 20% of the Maximum Shear stress in the bond-line. The lowest shear stress element was located in the middle (through the depth) of the bond-line as shown in Figure 51.

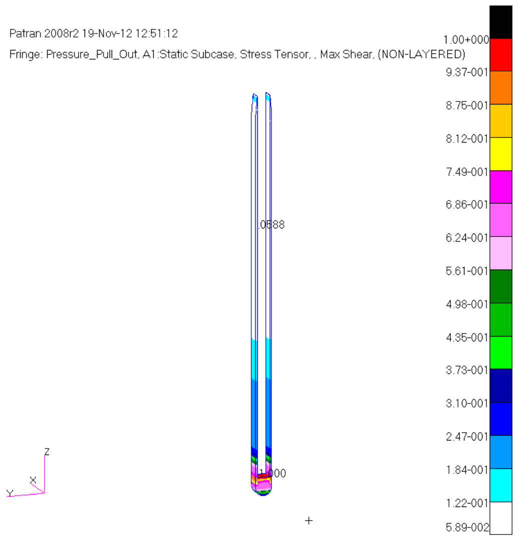

Baseline (Max Shear =1.000)

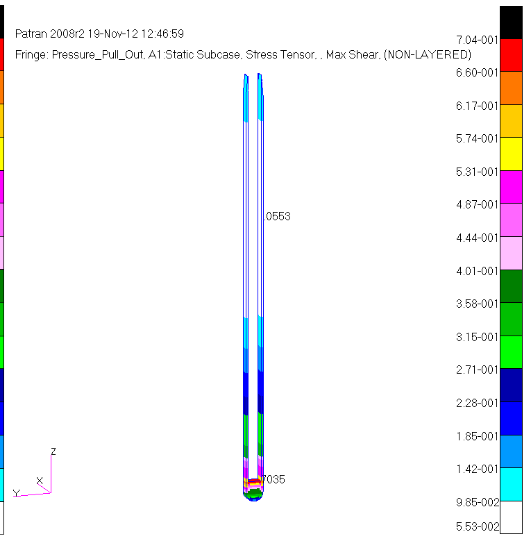

Overlap (Max Shear =0.704)

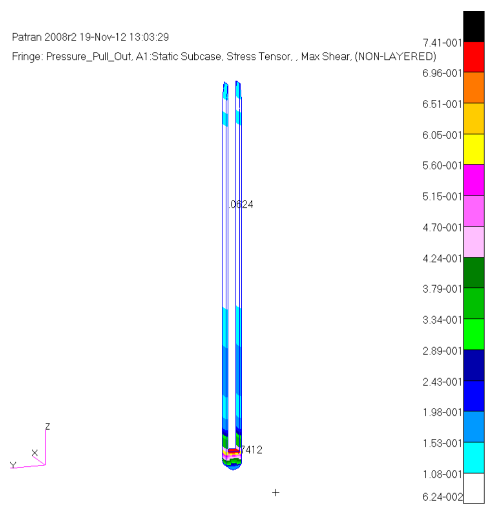

Unidirectional (Max Shear =0.741)

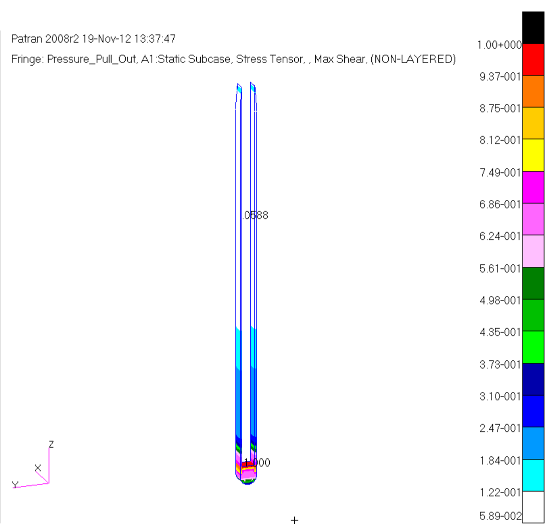

Pressure Intensifier (Max Shear =1.000)

Figure 51 Normalized Maximum Shear stress in the adhesive

3.3.3. Web Laminate

The Pi-Joint is very weak in resin-dominated properties, especially the web under the given loading conditions. Of course, this assumption will be validated through testing. For now only resin-dominated properties will be analyzed. As shown in the Figure 52, the highest out of plane stress in the joint was located in the middle (through the depth) of the web at the root of the joint. This behaviour was expected.

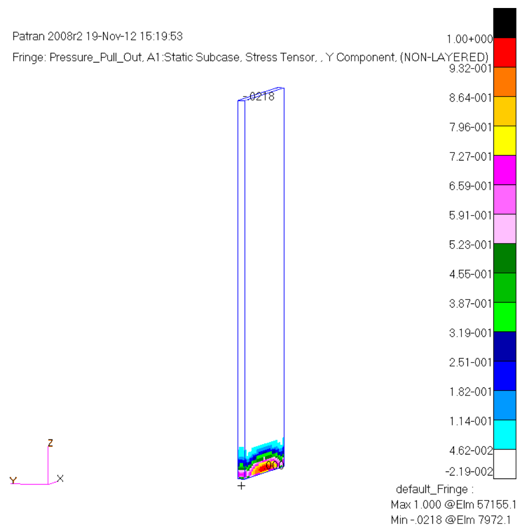

Baseline (Out of Plane Stress =1.000)

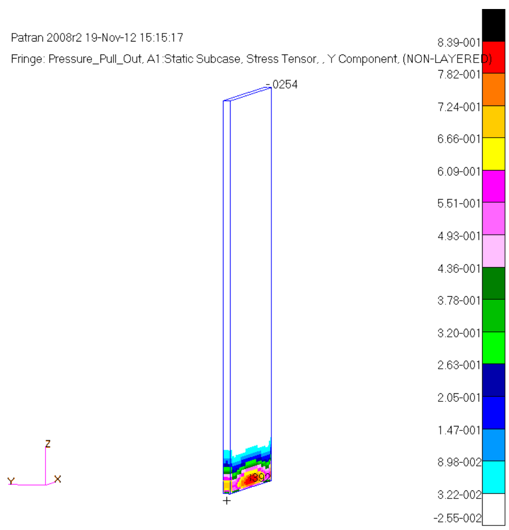

Overlap (Out of Plane Stress =0.839)

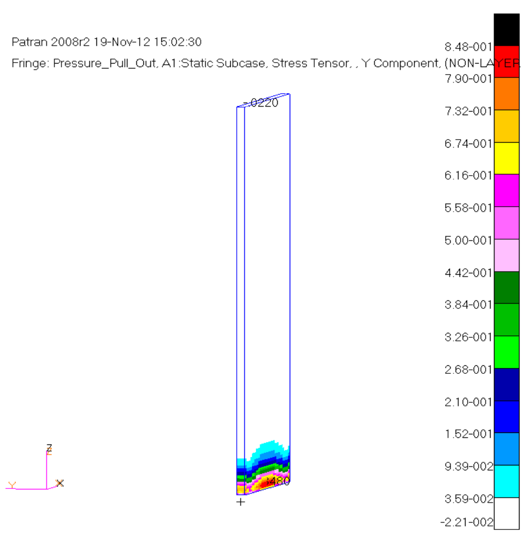

Unidirectional (Out of Plane Stress = 0.848)

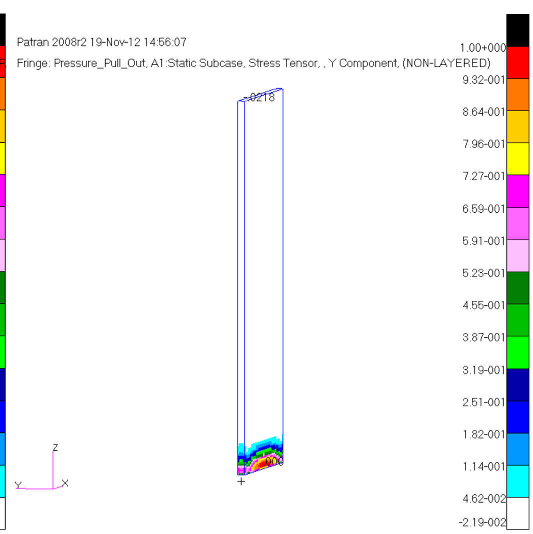

Pressure Intensifier (Out of Plane Stress =1.000)

Figure 52 Normalized out of plane stress in the web laminate

When the outward load is applied in the direction of web, the load transfer to the skin bends the skin, as shown in Figure 49. The upper surface of the skin was in tension and the lower section of the skin in compression. The web and the preformed Pi were cured to the upper surface of the skin; therefore, the web and the preformed Pi were in flat-wise tension. Any small delamination within the web laminate would make the joint unstable under the applied load and cause catastrophic failure in the joint.

3.3.4. Skin Laminate

The other section in the joint where out of plane stresses were critical was the skin. Since the applied load (tension) was perpendicular to the skin, any resin dominated-properties failure under the preform Pi would trigger a catastrophic failure in the joint. As it is seen in Figure 53, the highest loaded region in the skin laminate in the out of plane direction was under the preformed Pi for the Baseline configuration. Of course for the different configurations, the stiffness of the joint was somewhat different so as the location where the highest out of plane stress was located. This is because the locations where the highest out of plane stress happened were under the preform Pi and the end of the run-out of the preform Pi on the skin. The out plane stress in these two locations were comparable.

Under the preform Pi the normalized stress for the Overlap configuration was 0.725 and 0.6038 for the Unidirectional. This behaviour was expected since the stiffness of the preform Pi for the Overlap and Unidirectional was higher compared to the other two configurations. The shear load from the web was transferred to the skin over the larger area rather than been dumped directly at the root of the Pi-Joint.

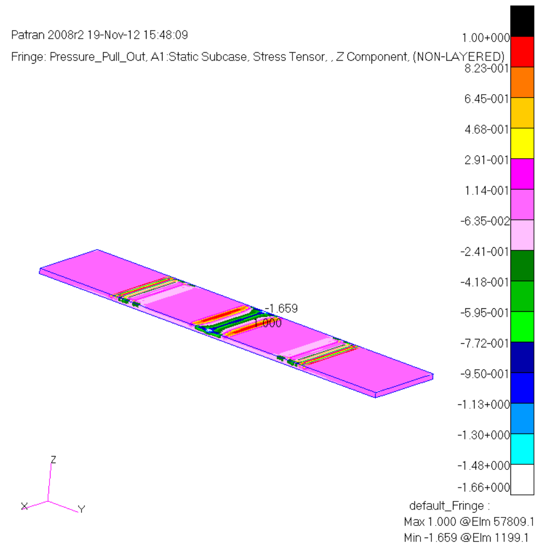

Baseline (Out of Plane Stress =1.000)

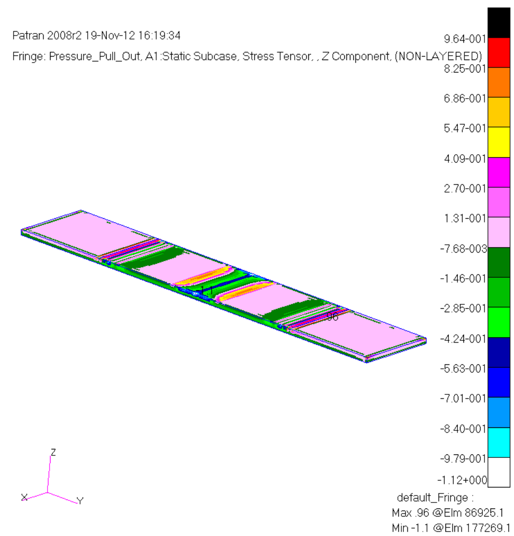

Overlap (Out of Plane Stress =0.964)

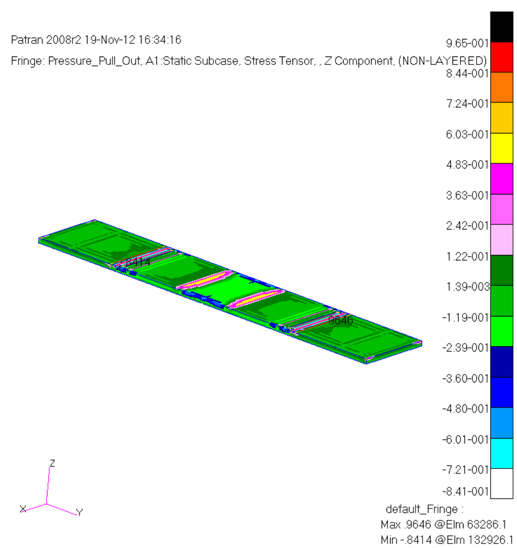

Unidirectional (Out of Plane Stress = 0.965)

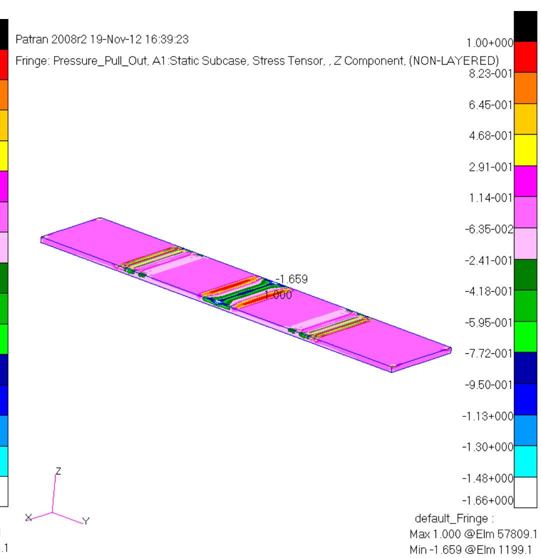

Pressure Intensifier (Out of Plane Stress =1.000)

Figure 53 Normalized out of plane stress in the skin laminate

3.3.5. U-Section Laminate

This section of the laminate was divided into two segments: a vertical segment and a curved segment.

3.3.5.1. Vertical Segment

The vertical segment of the joint had behaviour similar to the web laminate. For more details please refer to Section 3.3.3. Out of plane stresses in this section of the laminate is shown in Figure 54.

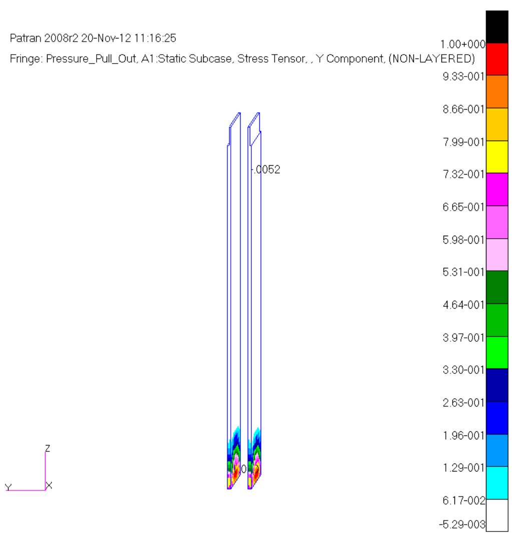

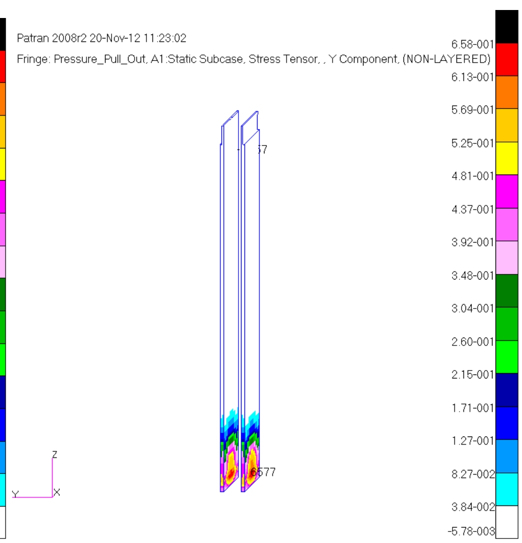

Baseline (Out of Plane Stress =1.000) Overlap (Out of Plane Stress =0.658)

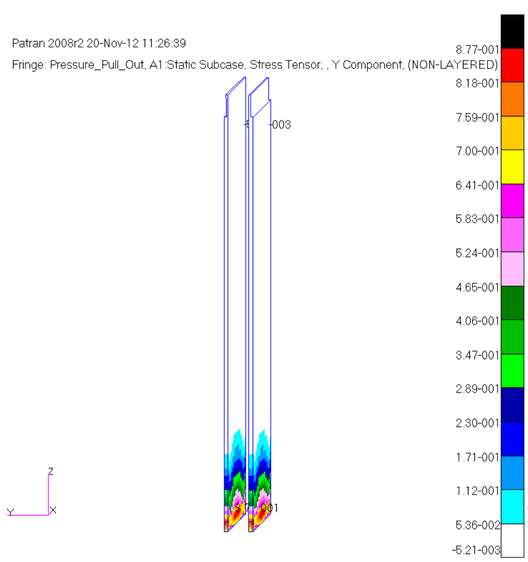

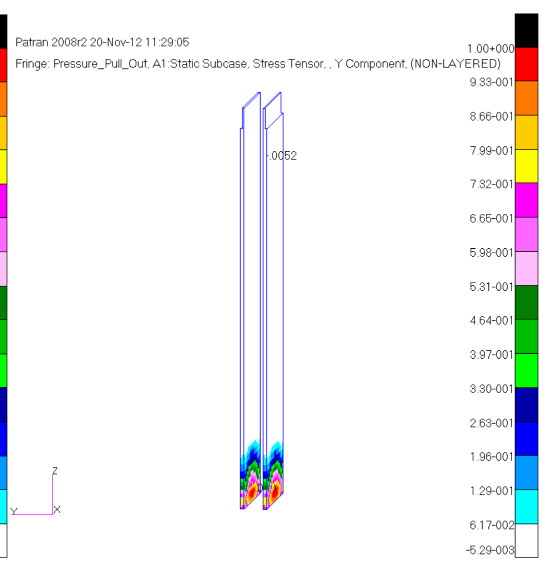

Unidirectional (Out of Plane Stress = 0.877) Pressure Intensifier (Out of Plane Stress =1.000)

Figure 54 Normalized out of plane stress in the U-Section laminate in the vertical segment

3.3.5.2. Curved Segment

A considerable percentage of the load was transferred at the end of the web. This is a normal behaviour for lap joints. However, the stiffness of the adhesive at the end of the web was considerably lower than the shear stiffness all along the bond-line. Although there is the tendency to transfer a larger fraction of the load from the end of the web to the curved segment of the U-Section laminate, the U-Section laminate stresses were very low. As the stiffness of the preform Pi increased, the stress in the curved segment of U-Section laminate is decreased, see Figure 55.

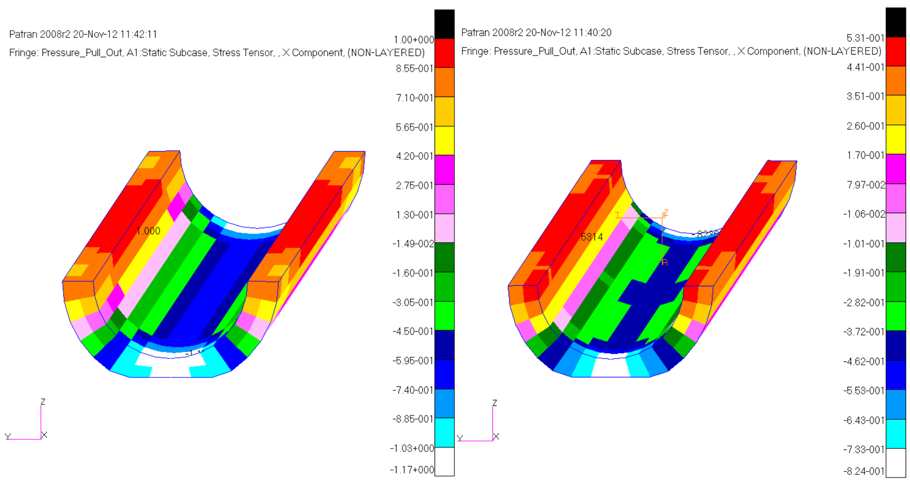

Baseline (Out of Plane Stress =1.000) Overlap (Out of Plane Stress =0.531)

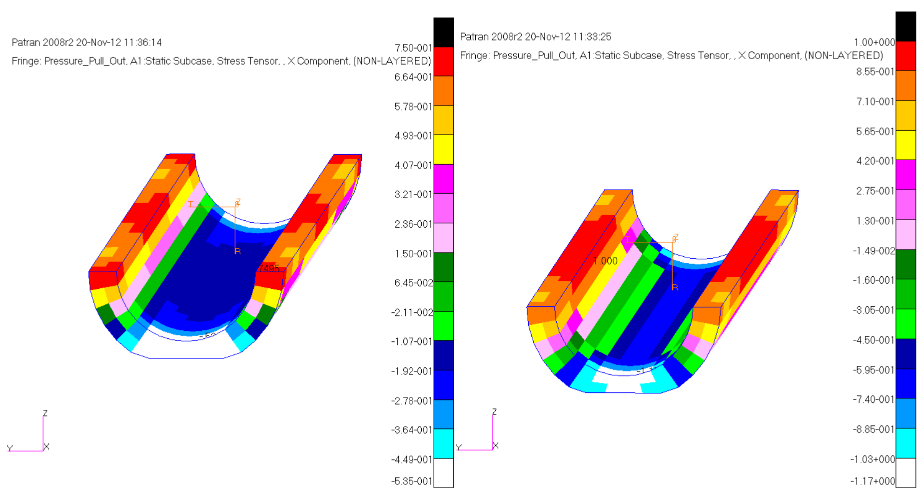

Unidirectional (Out of Plane Stress = 0.750) Pressure Intensifier (Out of Plane Stress =1.000)

Figure 55 Normalized out of plane stress in the U-Section laminate in the curved segment

3.3.6. L-Section Laminate

This section of the preformed Pi was divided into three segments: the vertical segment, the curved segment and the horizontal segment.

3.3.6.1. Vertical Segment

This section of the joint behaved like the web. The Vertical Segment of the preformed Pi was very weak in resin-dominate properties.

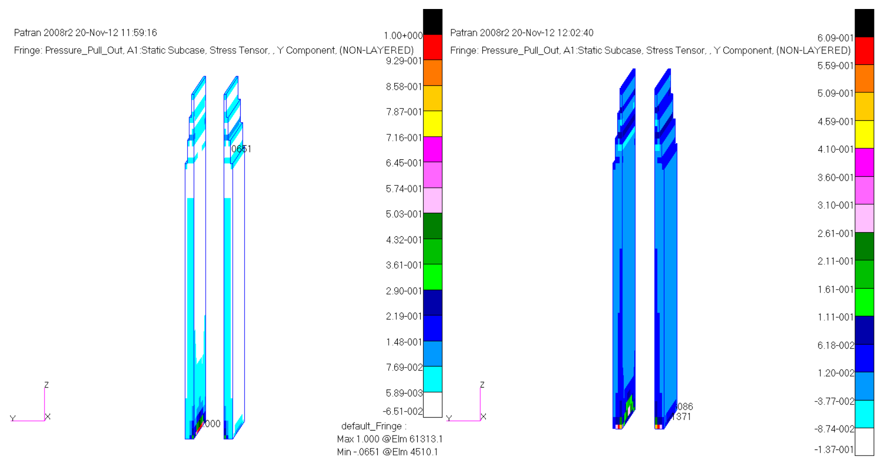

Baseline (Out of Plane Stress =1.000)   Overlap (Out of Plane Stress =0.531)

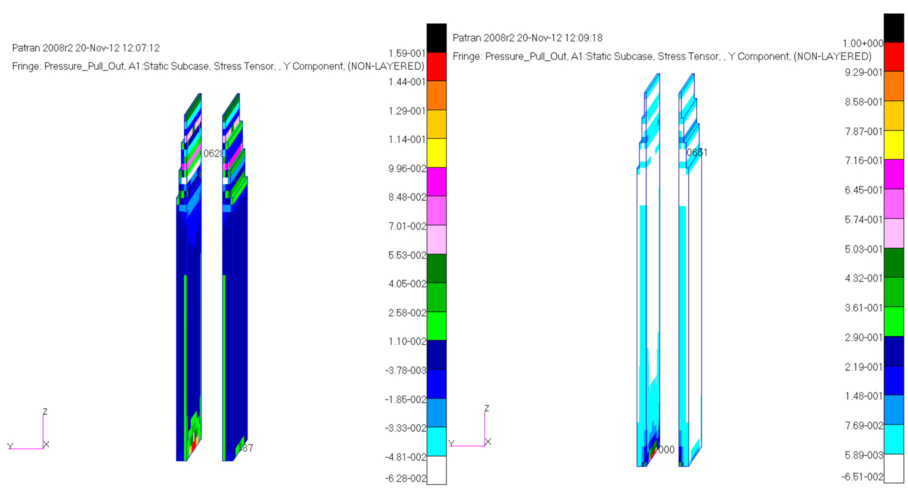

Unidirectional (Out of Plane Stress = 0.159) Pressure Intensifier (Out of Plane Stress =1.000)

Figure 56 Normalized out of plane stress in the L-Section laminate in the Vertical Segment

At this point only resin-dominated properties will be analyzed. As shown in Figure 56, the highest out of plane stress in the joint was located in the middle (through the depth) of the web at the root of the joint. This behaviour was expected.

3.3.6.2. Curved Segment

This section of the joint is the most important laminate. This section was highly loaded and the load level was very close to the failure. For this section geometry, any small variation in the radius would affect the stress concentration and ultimately the strength of the joint. The normalized stress shown in Figure 57 was flat wise tension in the laminate. It can be seen in Figure 57 that most of the load was transferred to the skin through the lower section curvature laminate. Any variation in the radius in this section can be critical for the joint. The Overlap configuration had only 85% of the Baseline configuration stress but of course the stiffness was considerably higher in the section. It can be seen in Figure 57 that the value of the stress was more distributed in the Overlap configurations. Since the radius was the largest in the Unidirectional configuration, it was expected that the normalized stress in Unidirectional configuration to be the lowest of the all, which was 51%.

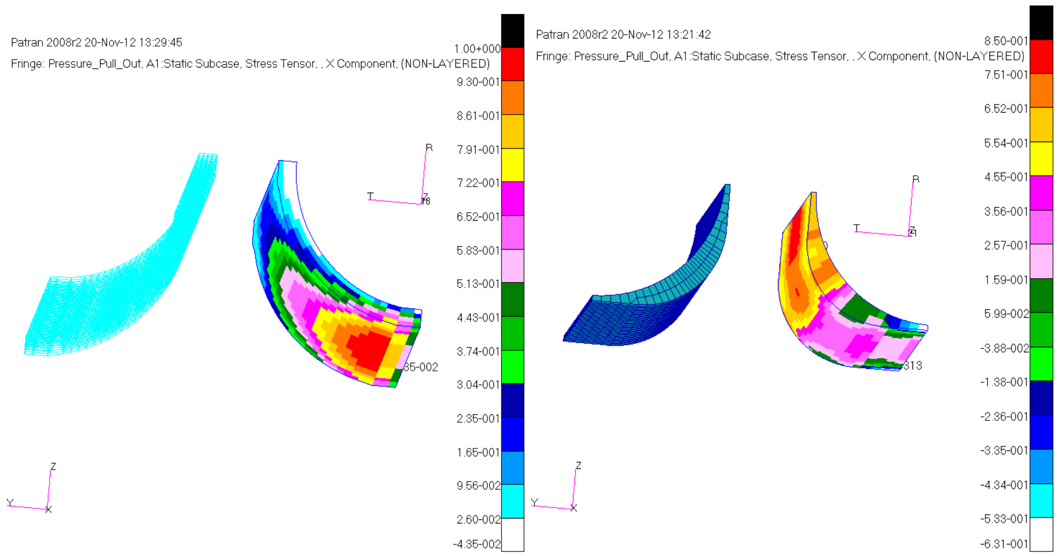

Baseline (Out of Plane Stress =1.000)   Overlap (Out of Plane Stress =0.850)

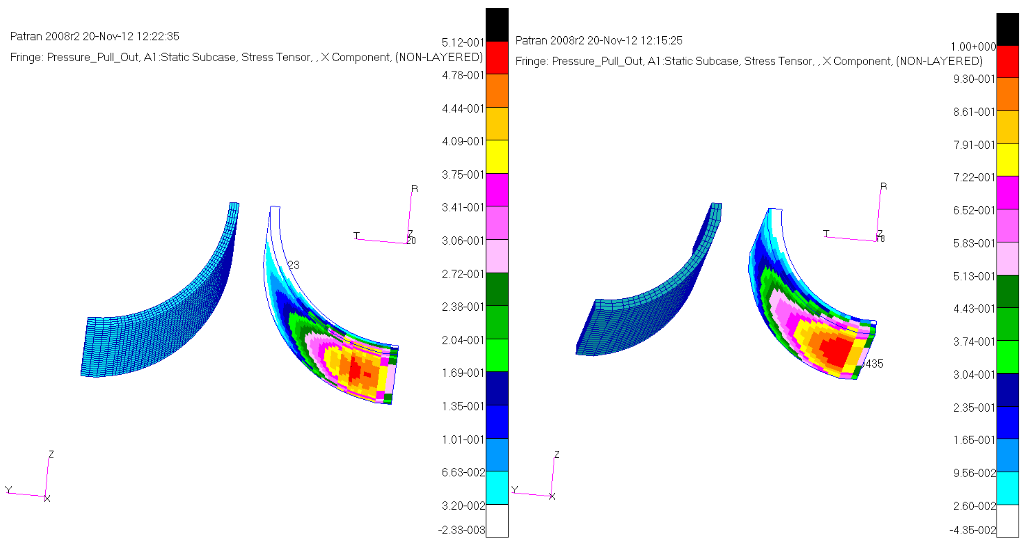

Unidirectional (Out of Plane Stress = 0.512) Pressure Intensifier (Out of Plane Stress =1.000)

Figure 57 Normalized out of plane stress in the L-Section laminate in the Curved Segment

3.3.6.3. Horizontal Segment

This section of the laminate behaved like to the skin. This segment is another location in the joint where out of plane stress is critical. Since the applied load (tension load) was perpendicular to the laminate, any resin dominate-property failure under the preform Pi would trigger a catastrophic failure in the joint. As it is seen in Figure 58, the highest loaded region in this section of the laminate in the out of plane was under the preformed Pi.

Under the preform Pi the normalized stress was 0.531 for the Overlap configuration, 0.750 for Unidirectional and 1.000 for Pressure Intensifier. This behaviour was expected since the stiffness of the preform Pi for the Overlap and Unidirectional was the highest compare to the other two configurations; therefore, the shear load from the web was transferred to the skin over a larger area.

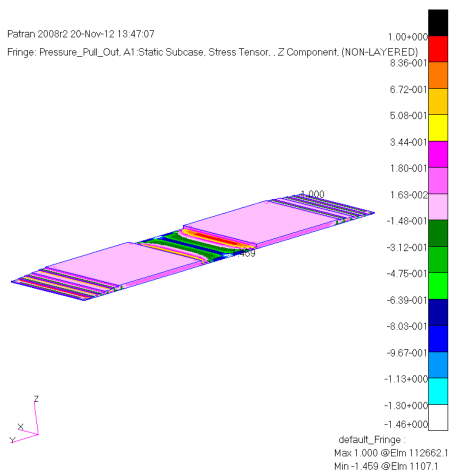

Baseline (Out of Plane Stress =1.000)

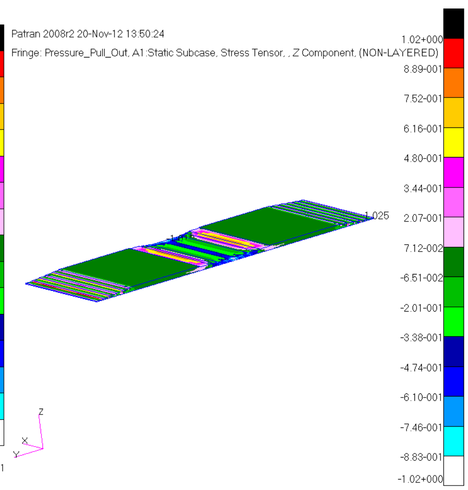

Overlap (Out of Plane Stress =0.531)

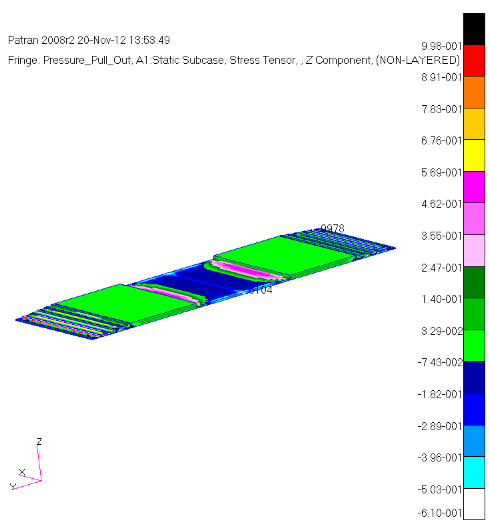

Unidirectional (Out of Plane Stress = 0.750)

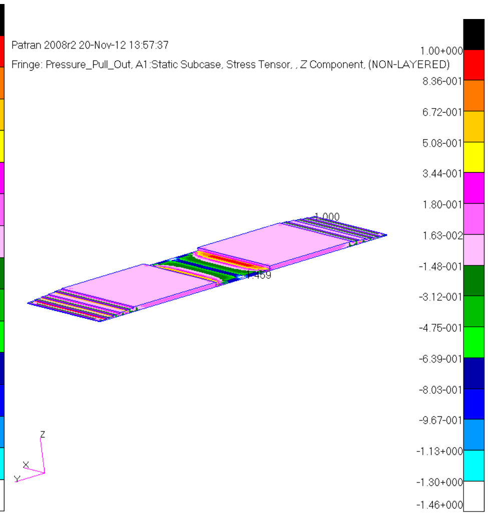

Pressure Intensifier (Out of Plane Stress =1.000)

Figure 58 Normalized out of plane stress in the L-Section laminate in the horizontal segment

3.3.7. Resin Rich Area

The resin rich area was section is another location in the joint where there was a considerable percentage of load transfer from the web to the skin. Any variation from the Baseline configuration is expected to have a pronounced effect on the behaviour of the joint. Since the upper portion of the skin laminate was in tension, the resin rich area was also in tension. Any failure in this region is expected to be due the flatwise tension between the resin and the adjacent laminate or within the resin. In the Baseline configuration the value of maximum principle stress was similar to the stress in the Y-Direction in global coordinate system. Moreover, the Maximum Principle stress did not represent the flatwise stress in the filler of the Unidirectional configuration. Therefore, the stress in the Y-Direction is depicted in Figure 59. As it is seen in this figure, the Overlap configuration had only 28.7 percent the stress of Baseline configuration in the resign rich area. On the other hand, the resin rich cross section area in the Overlap configuration is the smallest among the configurations. Since the load transfer through the resin reach area is function of level stress and the cross section area, there was not a considerable load transfer from the web to the skin through the resin reach area.

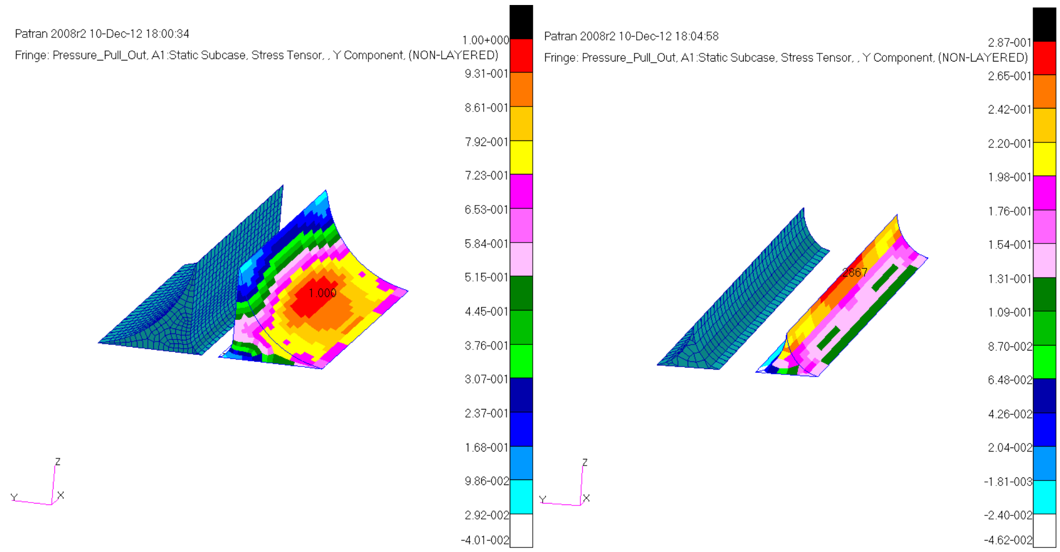

Baseline (Out of Plane Stress =1.000) Overlap (Out of Plane Stress =0.287)

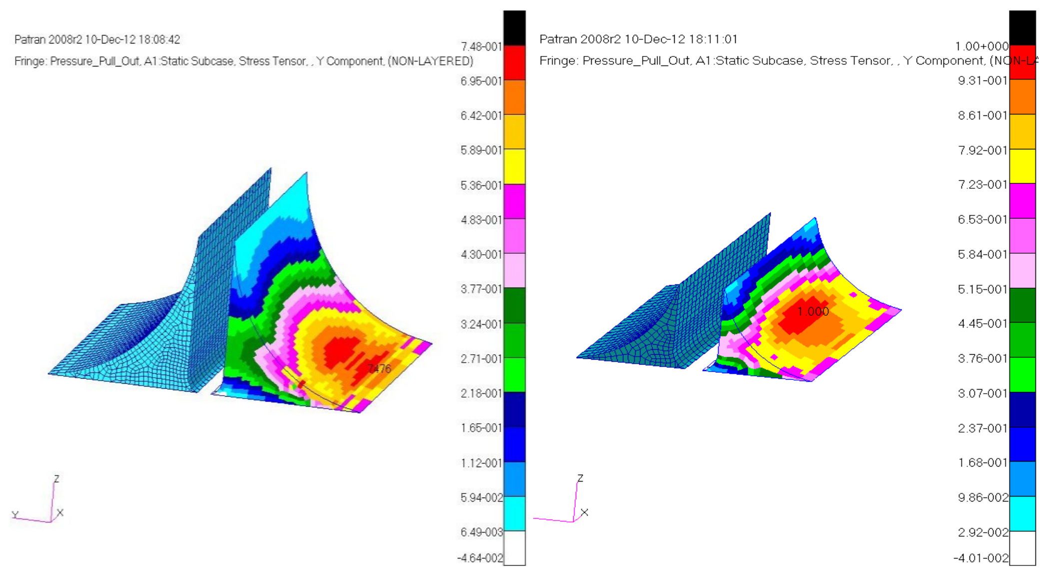

Unidirectional (Out of Plane Stress = 0.748) Pressure Intensifier (Out of Plane Stress =1.000)

Figure 59 Normalized stress in Y-Direction of the global coordinate system in the resin rich area

As shown in Figure 59, the Unidirectional configuration had 74.8 percent the stress of Baseline in the resign rich area. Although the stress was less in this section, because the cross section area was larger compared to the Baseline there was more load transfer from the web to the skin through this section. For the

Unidirectional configuration, the manufacturing conformity in this section of the joint was paramount for the strength of the joint.

The behaviour of the Pressure Intensifier configuration was similar to Baseline configuration because the models had the similar radii.

In summary, it is found that the Overlap Configuration had lower stresses in each segment of the laminate compared to the Baseline configuration. The Unidirectional configuration had the second lowest stress in most cases. Based on the analysis it is expected to that the strength of the Unidirectional configuration to be the second highest. However, due to the porosity in the laminate the strength of the Unidirectional configuration is the lowest.

Chapter 4.

Mechanical Testing of the Pi-Joint

Quality control during manufacturing and FEM simulation of the part do not necessary ensure the strength of the part. There are many factors in the design that are idealized in an FEM simulation, most of which have an effect on the final results. To ensure the reliability and conformity of the joint, testing is crucial. In this chapter the test objective and procedure of the Pi-Joint specimens are described.

4.1. Objectives and Test Plan

The objective of performing mechanical testing was to experimentally obtain the pull off strength of the Pi-Joint. The actual boundary conditions of the test were similar to those simulated in FEM.

The specimens were examined to ensure there were no unexpected embedded manufacturing flaws. The specimens were in contact with the test fixture simulating simply support boundary condition at the two extremities of the skin as shown in Figure 60. The web was clamped at the top extremity with MTS grip and a tension load was applied on the web to pull off the web off the preformed Pi section. The specimen was allowed to translate (left-to-right) on either side. It was not expected that the joint would slide to the side. However, in case of misalignment or an offset load, the sliding force was reacted by the friction between the skin laminate and the test fixture. Due to the nature of the numerical analysis, the boundary conditions applied on the FEM model and the boundary conditions on the test specimens slightly differed. For example, it was essential to fix one side of the skin at three degrees of freedom in the FEM simulation, but for test purposes it was desirable to fix the skin in translation in the direction of the applied load to the ensure a symmetric loading condition of the joint compared to the mid-line. It was important to ensure the applied load and the boundary conditions on the specimen were similar for both the FEM simulation and the experimental testing. As shown in the simulation section, Chapter 3, the first onset of failure was considered as the failure load of the specimen, however the test continued until the specimen could no longer carry load (evident destruction of the specimen was detected at that point).

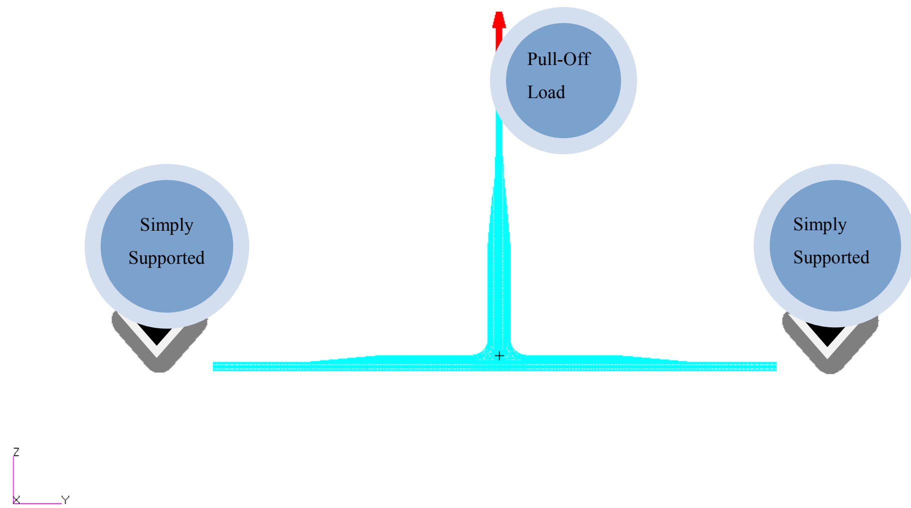

Figure 60 Boundary conditions of the test specimen (Repeated as Figure 45)

4.2. The Test Machine

The test machine was a displacement based tabletop electromechanical test frame (MTS Insight 5) that has two load cells of 5000 [N] and 500 [N]. The test machine was equipped with an extensometer to measure the strain of the specimen and had different testing fixture and grips to clamp and hold the specimens firmly and securely. The clamp for the MTS machine was used to clamp the web at the top. At the bottom a bolt was used to secure the test fixture to the MTS machine.

4.2.1. The setting of the Machine

All the specimens were tested under identical testing conditions. The rate of the pull-off load was 5.0 cm per minute. The specimens were loaded to approximately 5 [N] then the machine was reset to zero. A very small pre load was applied to ensure the specimens were not loose in the testing fixture at the start of the test. To end the test, the operating load was set to 10% of the applied peak load for each specimen. The final failure of the joint was sudden (brittle failure) and the crack became unstable, causing the web to separate from the skin.

4.2.2. The Test Fixture

Due to the shape of the Pi-Joint and loading direction, a specific test fixture, shown in Figure 61, was designed. The test fixture held the test specimen to simulate realistic boundary conditions for the joint.

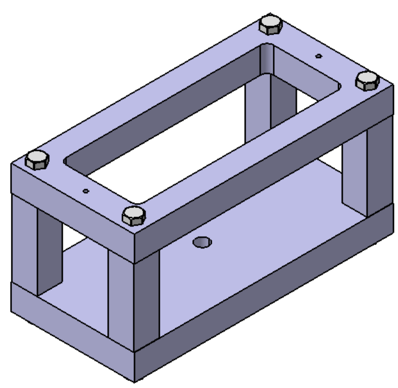

Figure 61 Test Fixture

The fixture legs were made of 1006-1020 carbon steel, the strength of the material is 372.3 MPa. The upper and lower housing of the fixture were made of Aluminum 2024-T3 plate. A simple strength analysis was conducted to ensure the text fixture would not fail or deform under the applied load.

The applied load was tension in the web, which exerted pull off load in the preformed Pi and out of plane bending in the skin. It was important to apply the load evenly in the web to ensure the stress applied to the preformed Pi was uniform and not concentrated on one side, see Figure 62. If the load was not uniform then there would be a premature failure lower than the estimated strength.

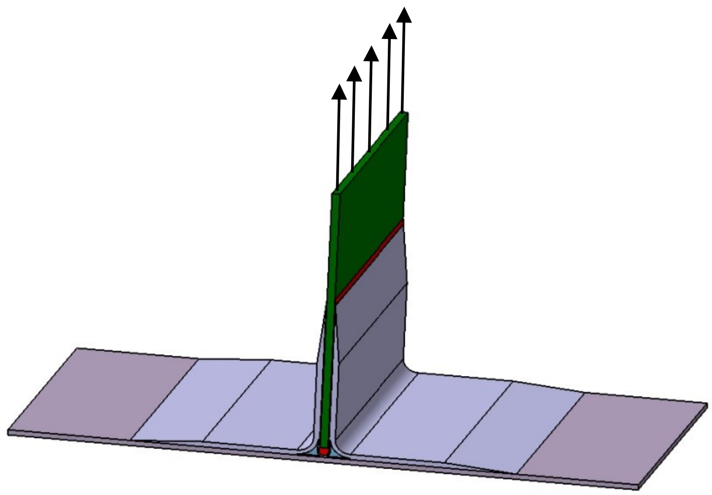

Figure 62 Uniform applied load on the web.

4.3. Mechanical Test Results

Four samples per configuration were tested to ensure repeatability in the behaviour of the specimens under the applied load. The results were normalized based on the separation displacement for the Baseline configuration, X-Axis, and the peak strength for the Baseline configuration, Y-Axis. The slope of the load-displacement curve represented the stiffness of the joint.

4.3.1. Baseline Configuration

As the displacement was increased, the load reacting on the web linearly increased up to 30%. The slope of the load-displacement curve was 24.66

[N/mm]. After 30% of the displacement is reached, a small drop in the load was accompanied by "ping-sound". As shown in Figure 63, the slope of the load-displacement curve was reduced.

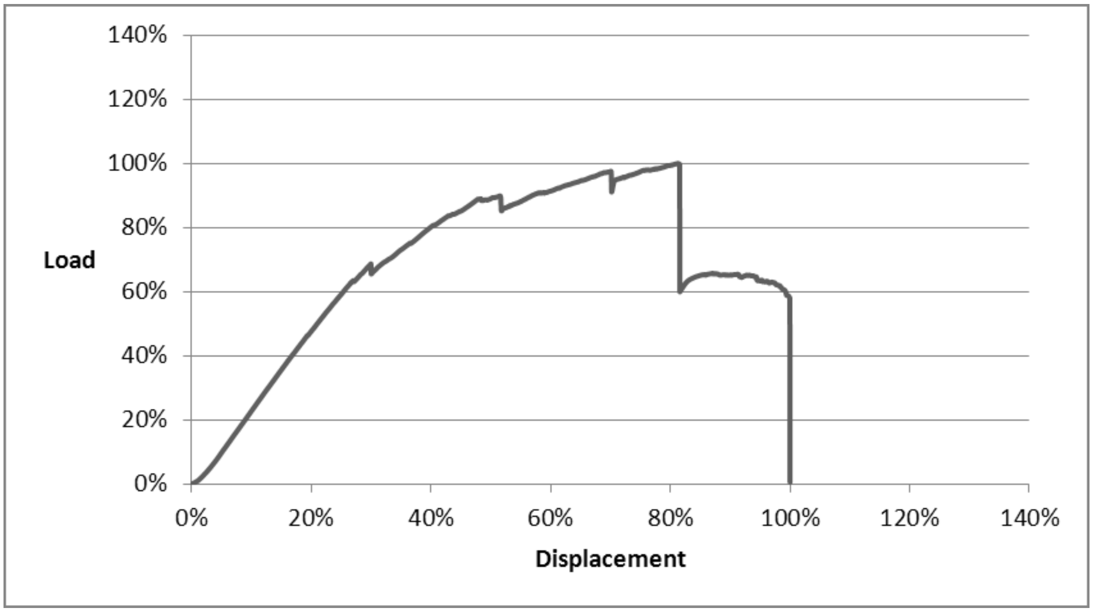

Figure 63 Normalized load displacement curve for the Baseline specimen

Similar behaviour was observed at normalized displacements of 50% and 70%. The ultimate strength of the joint was at a normalized displacement of 80%. At this point, there was a sudden drop in the load accompanied by a cracking sound. By that point the joint could only take 60% of the maximum load. After that the load bearing capability was almost constant until the total separation of the joint.

4.3.2. Overlap Configuration

As the displacement was increased, the load reacting on the web linearly increased up to a normalized displacement of 30%, as shown in Figure 64. The initial slope of the curve was 30.16 [N/mm]. This result was 22.3% higher compared to the Baseline configuration. After 30% percent of the displacement, there was a small drop in the load accompanied by a "ping-sound". The slope of the load-displacement curve was then reduced as shown in Figure 64.

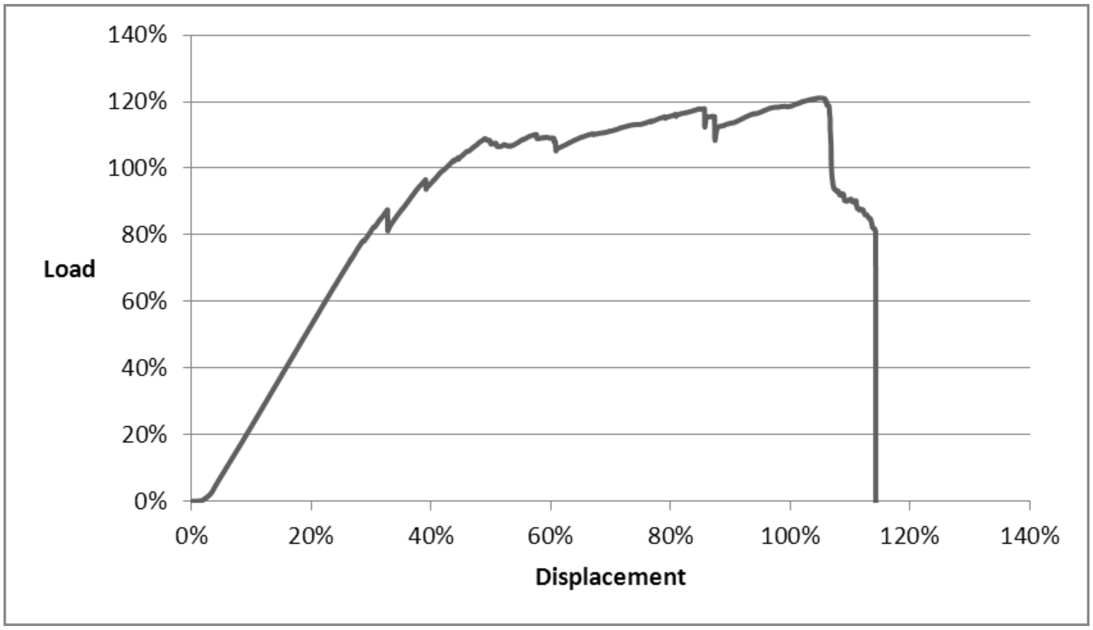

Figure 64 Normalized load displacement curve for the Overlap specimen

Similar behaviour was observed at normalized displacements of 50% and 105%. The ultimate strength of the joint is reached at 105% of displacement. At this point, there was a sudden drop in the load accompanied by a cracking sound. The load that the joint could bear was reduced even farther up to 115% of the displacement. At this point, there was a sudden failure and the joint separated from the skin.

4.3.3. Unidirectional Filler Configuration

For the Unidirectional filler configuration, the displacement was increased as the load reacting on the web linearly increased up to a normalized displacement of 35%, shown in Figure 65. The slope of the load-displacement curve was 25.56 [N/mm], or 3.6% higher compared to the Baseline configuration. The Unidirectional configuration is slightly stiffer than the Baseline but softer than the Overlap configuration. Between 35% to 40% percent of the displacement, there is a small drop in the load accompanied by a "ping-sound". However, as seen in

Figure 65, the slope of the load-displacement curve is considerably reduced after the first crack is initiated in the specimen.

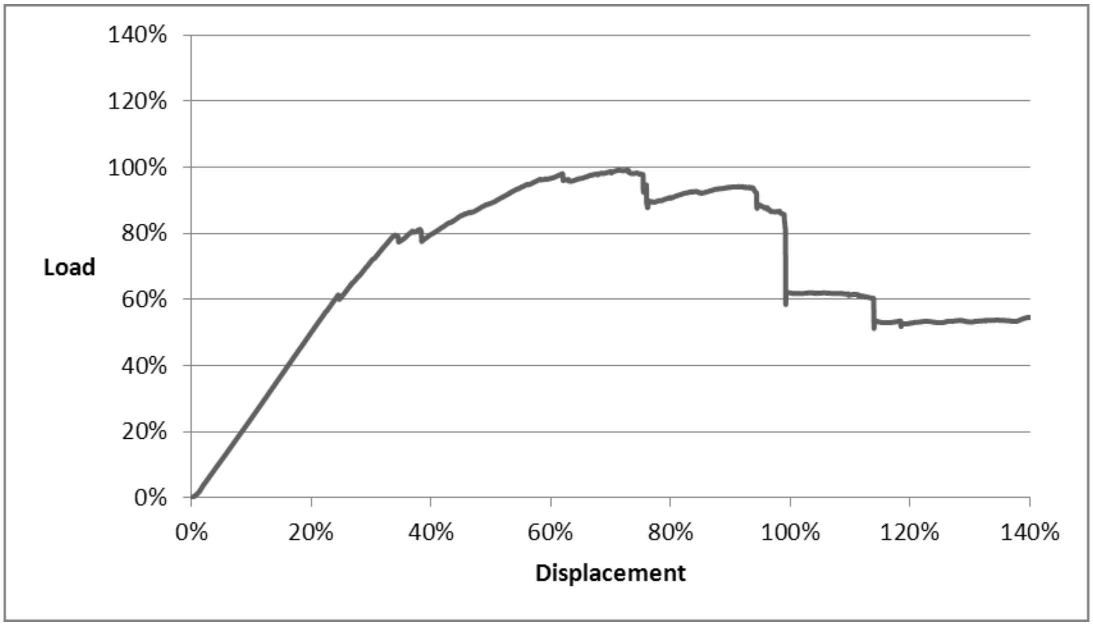

Figure 65 Normalized load displacement curve for the Unidirectional filler specimen

Similar behaviour was observed at normalized displacement of 75% and 95%. It was noted that the load was almost constant under large displacements for this configuration after the 95% displacement. Ultimately, the joint failed at a displacement about four times larger than the Baseline configuration. At this point the joint was able to carry about 60% of the load. It was observed that the final mode of the failure was compression in the skin, which is different than other configurations.

4.3.4. Pressure Intensifier Configuration

As the displacement was increased, the load reacting on the web is linearly increased up a normalized displacement of 40%. The slope of the load-displacement curve was 23.89 [N/mm]. At approximately 50% percent of the displacement, there was a sudden drop in the load accompanied by a "ping-sound". As seen in Figure 66, the slope of the load-displacement curve was reduced. Similar behaviour was observed at normalized displacement of 90%. The ultimate strength of the joint was reached at 90% of displacement. Finally at 95% of the displacement, there was a sudden drop in the load accompanied by a cracking sound and the joint was broken.

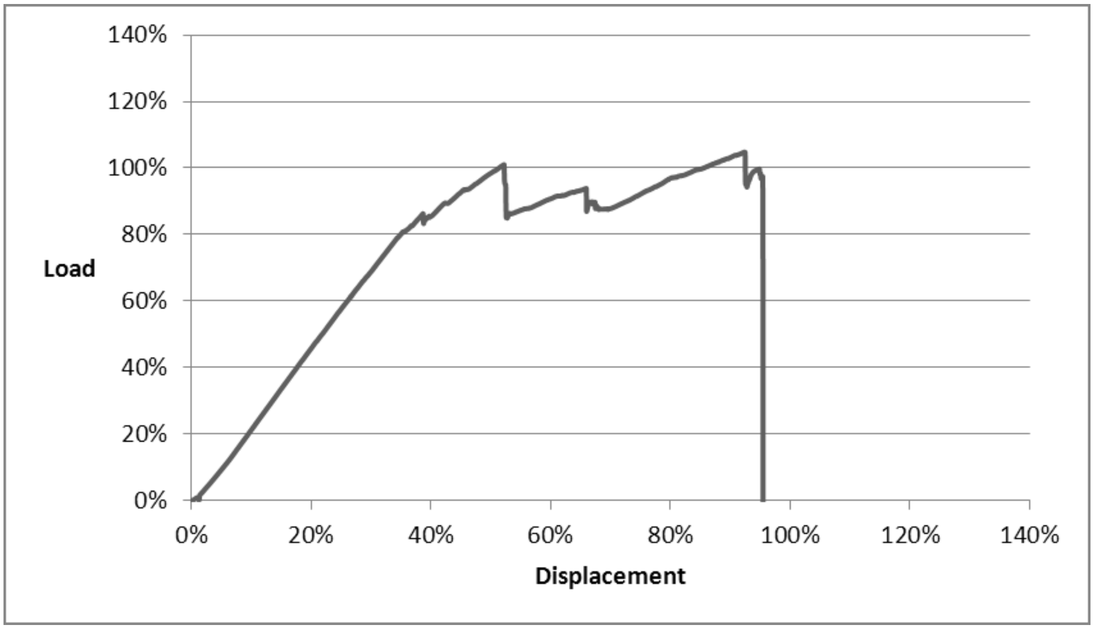

Figure 66 Normalized load displacement curve for the Pressure Intensifier specimen

4.3.5. Test Results Statistics

Usually higher level of porosity reduces the strength of the laminate. Stress concentration and lack of fibre support are the main reasons for the reduction in the laminate strength. Porosity in one of the reasons that would causes higher uncertainty in the laminate strength. Greater the standard deviation would result in a higher uncertainty in the strength of the joint, more specifically in the A-basis or B-basis allowable for the joint. In this section the standard deviation for different Pi-Joint configurations are calculated.

Of course reduction in the allowable due to large standard deviation is undesirable. In Table 5 the average failure load and standard deviation for each configuration are presented. The tabulated data presented here is based on four test specimens per configuration.

For the Baseline configuration, the average failure load was about 876 [N]. The standard deviation was 36 [N]. As it is shown in the Figure 70 to Figure 73, the ultimate strength of the joint was recorded about 16.5 [mm] of the displacement.

For the Pressure Intensifier configuration, the average failure load is about 892 [N]. The standard deviation is 36 [N]. As it is shown in the Figure 74 to Figure 77, the ultimate strength of the joint was recorded about 18.0 [mm] of the displacement. After the displacement of about 10.0 [mm], there is a considerable drop in the strength on the joint. The displacement had to be increased by 80% more to gain about 5% strength. Depending on the design, whether the design is a single load path or multiple load path, the ultimate strength of the joint can be considered at 18.0 [mm] of the displacement if the design is single load path or 10.0 [mm] if the joint is multiple load path, due the redistribution on the load in multi load path design. In this study, 18.0 [mm] of displacement is considered as ultimate strength on the joint.

For the Overlap configuration, the average failure load is about 1072 [N]. The standard deviation is about 59 [N]. As it is shown in the Figure 78 to Figure 81, the failure of the joint happened at 23 [mm] of the displacement but the ultimate strength of the joint was recorded about 21.5 [mm] of the displacement. Similarly to Pressure Intensifier configuration after 10.0 [mm] of the displacement there is a drop in the strength of the joint.

If the design is multi-load path, the ultimate strength of the joint could be considered at about 10.0 [mm] of the displacement. In this study, 21.5 [mm] of displacement is considered as ultimate strength on the joint because the overall strength of the joint (not the load transfer through the bond-line) is considered as a single load path design.

For the Unidirectional Filler configuration, the average failure load is about 865 [N], The standard deviation is about 57 [N], As it is shown in the Figure 82 to Figure 85, the ultimate strength of the joint was recorded about 11.0 [mm] of the displacement.

Configuration	Average Failure Load [N]	Standard Deviation [N]
Baseline	876.4	36.0
Pressure Intensifier	892.5	35.8
Overlap	1072.1	58.9
Unidirectional Filler	864.8	56.9

Table 5 Test Results Statistics

In this research study it was observed that the joints with higher porosity in at the root of the Pi-Joint have higher standard deviations. For example Overlap and Unidirectional Filler have porosity of 4.6% and 7.4% at the zone 4, section 2.6.2; moreover, the standard deviations for these two configurations are 59 [N] and 57 [N], correspondingly.

4.4. Observations during the Test

During the experimental testing of the specimens, there were some observations made that were of importance to the research study. These outcomes confirmed the validity of the FEM simulations. It has been previously noted that there was some manufacturing variability in the specimen causing a small variation in the test results. Moreover, it was observed that the first mode of failure for all the specimens was identical. The second mode of failure varied from one specimen to another. The analysis of the second mode of failure is out of scope of this study but the results are of interest, therefore they will be briefly addressed.

It was observed that the first mode of failure for most of the specimens was a delamination in the curved segment of the L-Section laminate as shown in Figure 67. This mode of failure corresponded to the FEM simulation analysis done in section 3.3.6.2.

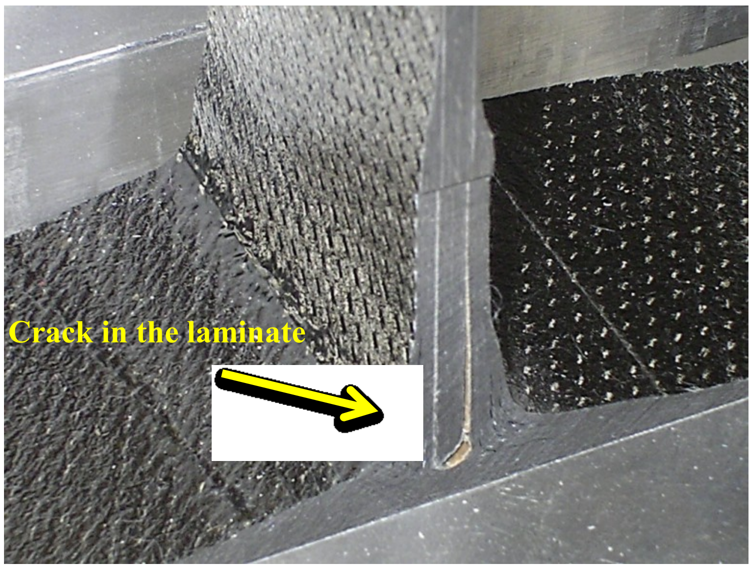

Figure 67 First mode of failure for the Overlap configuration

The second mode of failure for the Baseline, Overlap, and Pressure Intensifier configurations was a delamination of the preformed Pi to the skin laminate accompanied by a large deformation in the specimens, as shown in Figure 68.

The second mode of failure for the Unidirectional configuration was a failure in compression of the skin laminate, as shown in Figure 69. The failure of laminate in compression was accompanied by a large deformation in the specimens.

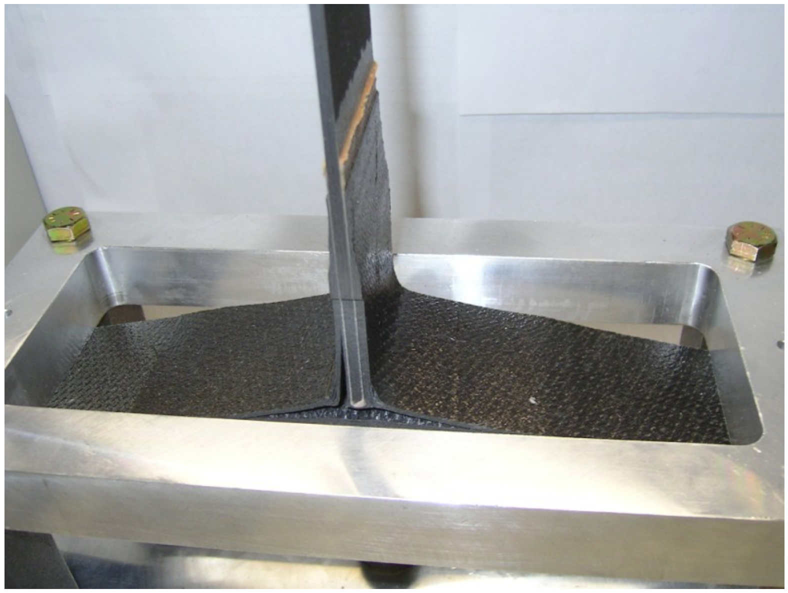

Figure 68 Second mode of failure for the Baseline, Overlap and Pressure Intensifier configuration

Figure 69 Second mode of failure for the Unidirectional configuration

Chapter 5.

Conclusions and Future Work

5.1. Summary and Conclusions

The present research study addressed the effect of design and manufacturing variation on the mechanical performance of a Pi-Joint. . The strength of composite parts is highly dependable on the manufacturing technique and design conformity. Hence, the objective of this work was to compare the effect of different manufacturing techniques on mechanical strength and to investigate the manufacturing challenges due to OOA process. The conclusion from this research study is described below:

1. **The porosity of Pi-Joint at the corner is very sensitive to different manufacturing techniques**

The Baseline configuration has the lowest porosity level of all the other configurations, as shown in Table 3. During the layup of the radius there is no extra step required to manufacture the Baseline configuration. From the manufacturing cost point of the view the Baseline configuration is preferred. Moreover, Baseline configuration results in a lower porosity level among all the configurations. Adding more material in the radius region of the Over-lap configuration causes a higher porosity level at the radius. Likewise, Unidirectional Filler configuration has the highest porosity level at the radius of Pi-Joint. It is recommended to manufacture Pi-Joints with no additional material, such as unidirectional filler, in the radius to reduce the porosity at the most critical section in the joint.

2. **The level of porosity does not have a direct relationship with the mechanical performance of the Pi-Joint**

Higher porosity causes a higher stress concentration in the laminate. There is a tendency to assume that higher porosity means lower laminate strength; it is counter intuitive to assume a part with higher porosity level is stronger. For example, in the Baseline configuration, the porosity is lower than the Overlap configuration but the Overlap configuration had the highest strength. The Unidirectional filler configuration had the highest level of porosity but the strength of the joint was similar to the Baseline configuration. High porosity at the radius translates to less compaction meaning a thicker laminate at the radius, causing a larger radius. Ultimately, a large radius translates to a smaller geometrical stress concentration at the radius yielding a stronger Pi-Joint. It cannot be assumed that Pi-Joint with the highest level of porosity is the weakest. The strength of Pi-Joint is a function of the level of porosity and radius obtained. This radius is function of compaction and porosity of the L-Section laminate.

3. **Different manufacturing techniques affect the stiffness of Pi-Joint**

The different manufacturing techniques of the four configurations had different resulting strength and/or stiffness. The Overlap configuration had the highest stiffness which was 22% higher than the Baseline, followed by the Unidirectional configuration which was 3.6% higher than the Baseline. In a multi-load path design, different stiffness in the load path affects the load distribution in the structure. In application of Pi-Joint in a multi-load path design, it is possible to redistribute the load based on the different manufacturing technique without any weight increase in the design.

5.2. Future Work

Further improvement can be made to the numerical model by including the strength of the laminate with the porosity at the radius in the FEM model. This requires the development of an experimental study to obtain the stiffness and strength of the laminate with the given percentage of porosity. These experimental studies could be done on flat specimens and the results can be extrapolated to the curvature at the radius of the Pi-Joint. Another topic of potential interest for Pi-Joints is the crack growth in the adhesive under static and fatigue loads. It is interesting to demonstrate the bondline at each side the web acts independently of each other. In other words, there is a crack arrest feature inherited in the design of Pi-Joint. Numerical study and experimental study can be performed to show this behaviour. Ultimately, a numerical or analytical tool can be developed to predict the rate of crack growth under pull-off and shear static and fatigue loads in the web. Also, an optimization study to reduce the weight and enhance the strength of the Pi-Joint can be investigated. Investigation of all these studies can bring us closer to a new generation of light and reliable joints used on primary aircraft structures.

LIST of REFERENCES

1. Scholz, D.B., Dost, E. F., Flynn, B. W, Ilcewicz, L. B., Nelson, K. M., Sawicki, A. J., Walker, T. H., *Advanced Technology Composite Fuselage - Materials and Processes*, R. 4731, Editor 1997, The Boeing Company: Seattle, Wanshington. p. 250.
2. Walker, T.H., Minguet, P. J., Flynn, B. W., Carbery, D. J., Swanson, G. D.,Ilcewicz, L. B., *Advanced Technology Composite Fuselage - Strucutral Performance.* 1997(4732): p. 101.
3. Hale, J., *Boeing 787 from the Ground Up*, in *Boeing.com/Commercial/Aeromagazine*2006.
4. Caudron, F., *A350 XWB Programme Update*, Airbus, Editor 2010.
5. Miracle, D.B., Donaldson, S.L., *Volume 21 Composites ASM International*. Vol. 21. 2004. 1184.
6. Tserpes, K.I., S. Pantelakis, and V. Kappatos, *The effect of imperfect bonding on the pull-out behavior of non-crimp fabric Pi-shaped joints.* Computational Materials Science, 2011. 50(4): p. 1372-1380.
7. Niu, M.C.Y., *Airframe Stress Analysis and Sizing*. Second ed1999: Conmilit Press Ltd.
8. Brot, A., *Assessing the Reliability of Fail-Safe Structures*, in *ICAF*2001: Toulouse.
9. Advani, S.G., Murat Sozer, E., *Process Modeling in Composite Manufacturing*2003: Marcel Dekker, Inc.
10. R. S. Dave, A.C.L., *Processing of Composites*, ed. W. Baker1999: Hanser.
11. G.G. Bond, J.M.G., G.L. Hahn, C. Bongiovanni and J. Boyd,, *Non-Autoclave Prepreg Manufacturing Technology*, in *40th SAMPE Fall Technical Conference*2008.
12. Abaris, Design and Analysis of Composite Strctural Joints, Rikard Heslehurst, 2006.
13. Russell, J.D., *Transitionaing Advanced Aerospace Technologies Through Cost and Risk Reduction*, A.F.R. Laboratory, Editor 2006: Ohio, United State of America.
14. Craig Collier, Phil Yarrington, and M. Pickenheim, *Analysis Methods used on the NASA Composite Crew Module (CCM).* American Institute of Aeronautics and Astronautics, 2008: p. 28.
15. Libin ZHAO, J.L., Tianliang QIN, Hai HUAN, *ANALYSIS OF COMPOSITE ADHESIVE-BONDED JOINTS.* International Conference on Composite Materials, 2009.
16. K.I. Tserpes, S.P., V. Kappatos, *The effect of imperfect bonding on the pull-out behavior of non-crimp fabric Pi-shaped joints.* 2010.
17. LIBIN ZHAO, T.Q., R. AJIT SHENOI, JIANYU ZHANG, XIANZHU LIANG AND HAI HUANG, *Strength Prediction of Composite P Joints Under Tensile Load.* Journal of Materials Science, 2010. **44**: p. 20.
18. Hitesh Kapoor, J.L.B.a.S.R.S., *Damage Detection in z-Fiber Reinforced, Co-Cured Composite Pi-Joint Using Pitch-Catch Ultrasonic Analysis and Scanning Laser Vibrometry.* Tech Science Press, 2010. **3**: p. 18.

19. F. Weyrauch, L.L., F. Strachauer, *AN INNOVATIVE APPROACH ON MODULAR JOINTS FOR CARBON FIBRE REINFORCED STRUCTURES.* 2012.
20. Russell, J.D., *Transitioning Advanced Aerospace Technologies trhough Cost and Risk Reduction.* Advanced materials, Manufacturing, and Testing Information Analysis Center, 2007. 1(3).
21. Hexcel, *Technical Fabrics Handbook*, 2010.
22. M. Brillant, *Out-of-Autoclave Manufacturing of Complex Shape Composite Laminates,* 2010.

APPENDIX

Raw Data:

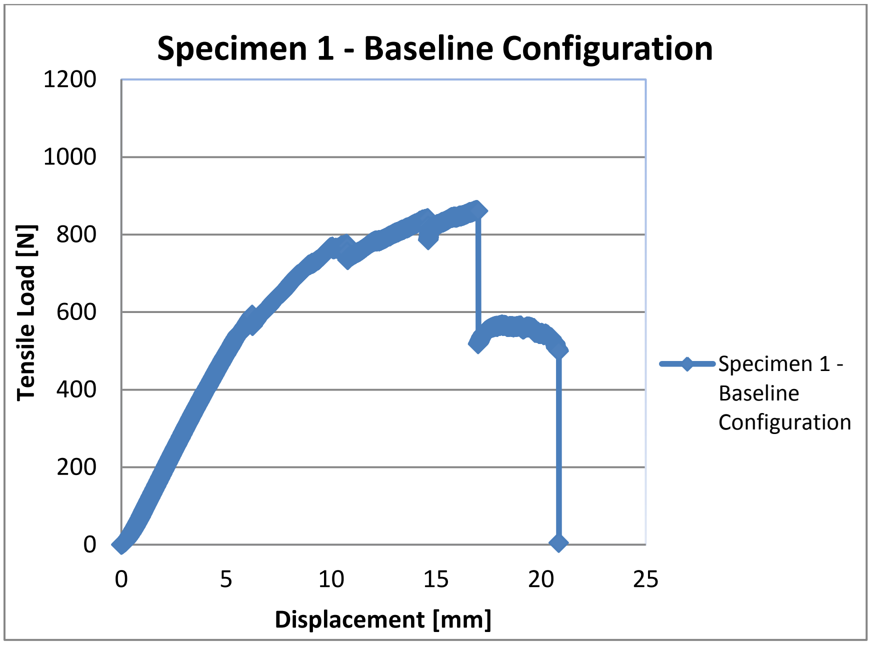

Figure 70 Load-displacement curve for Baseline specimen 1

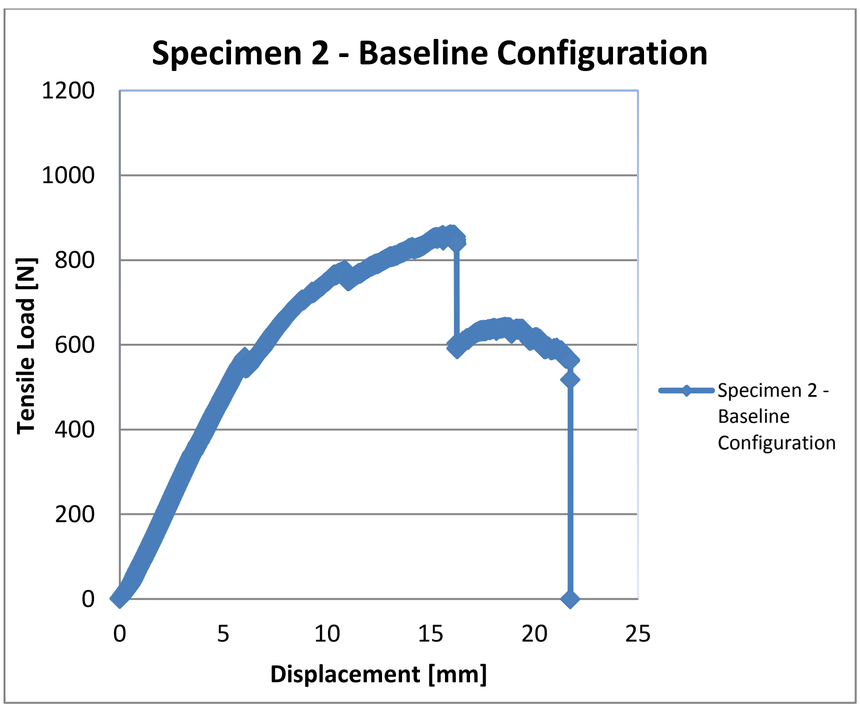

Figure 71 Load-displacement curve for Baseline specimen 2

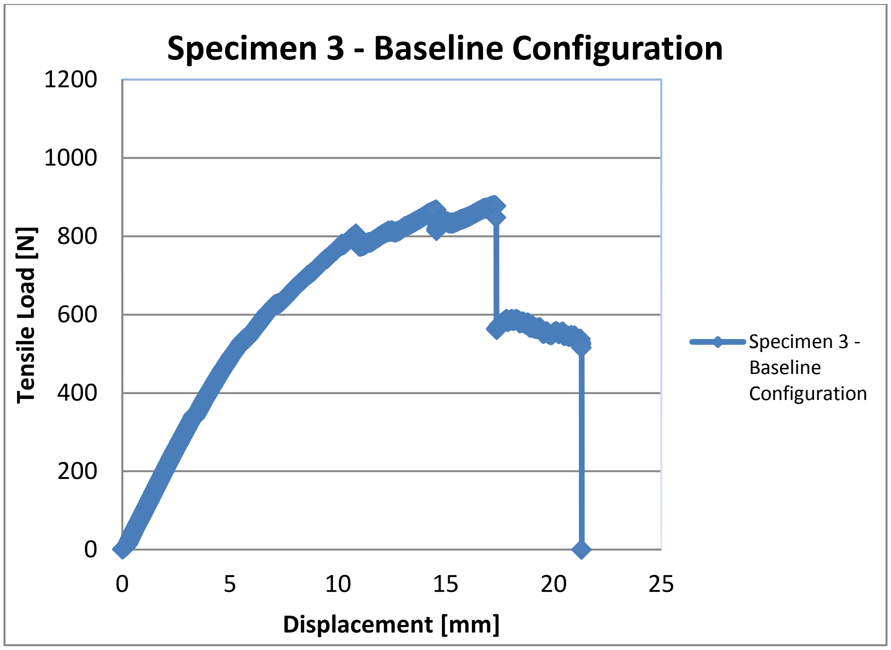

Figure 72 Load-displacement curve for Baseline specimen 3

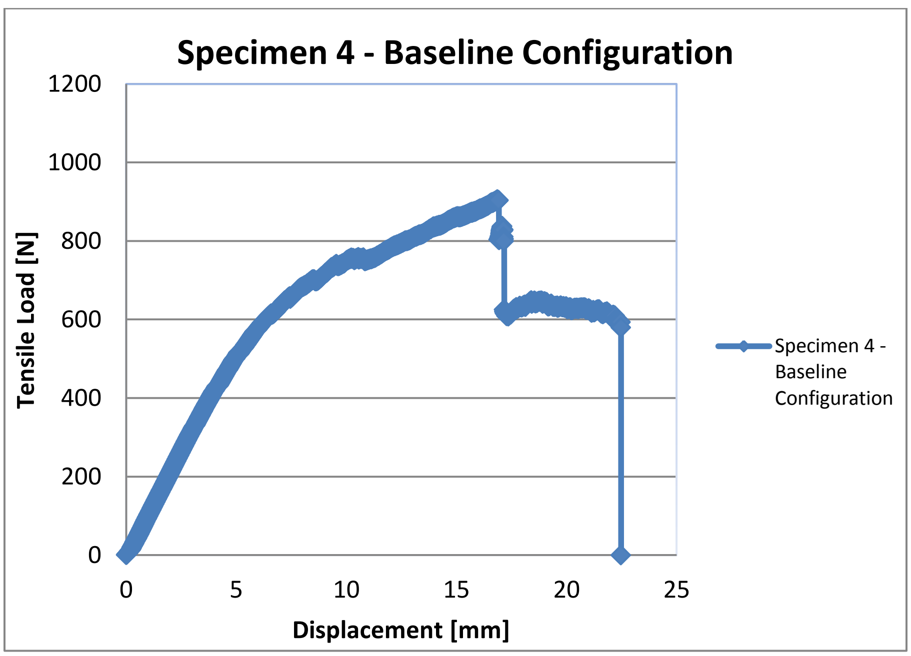

Figure 73 Load-displacement curve for Baseline specimen 4

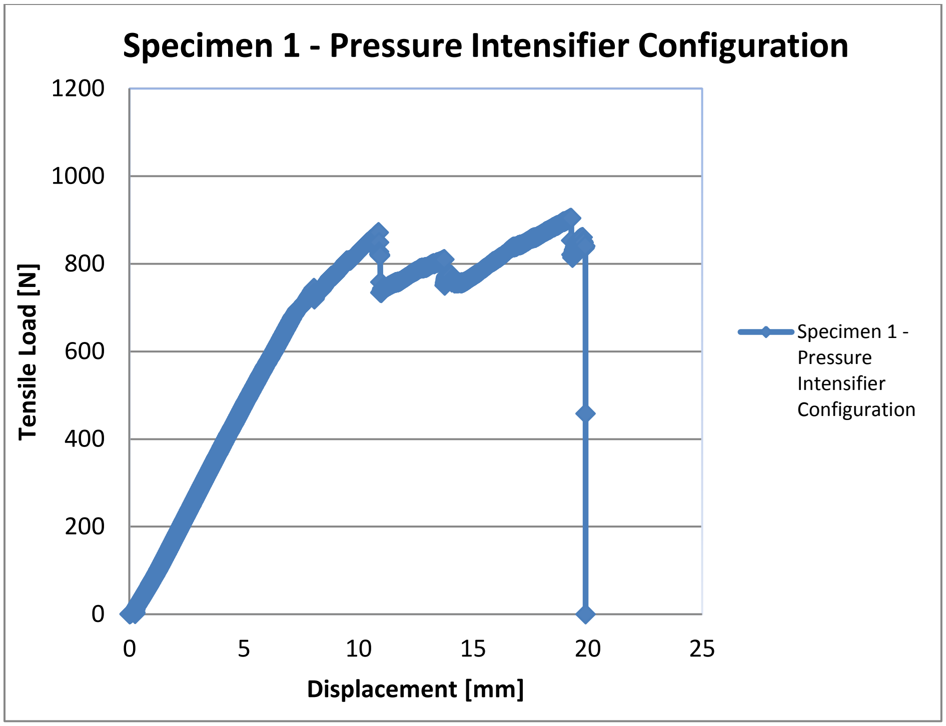

Figure 74 Load-displacement curve for Pressure Intensifier specimen 1

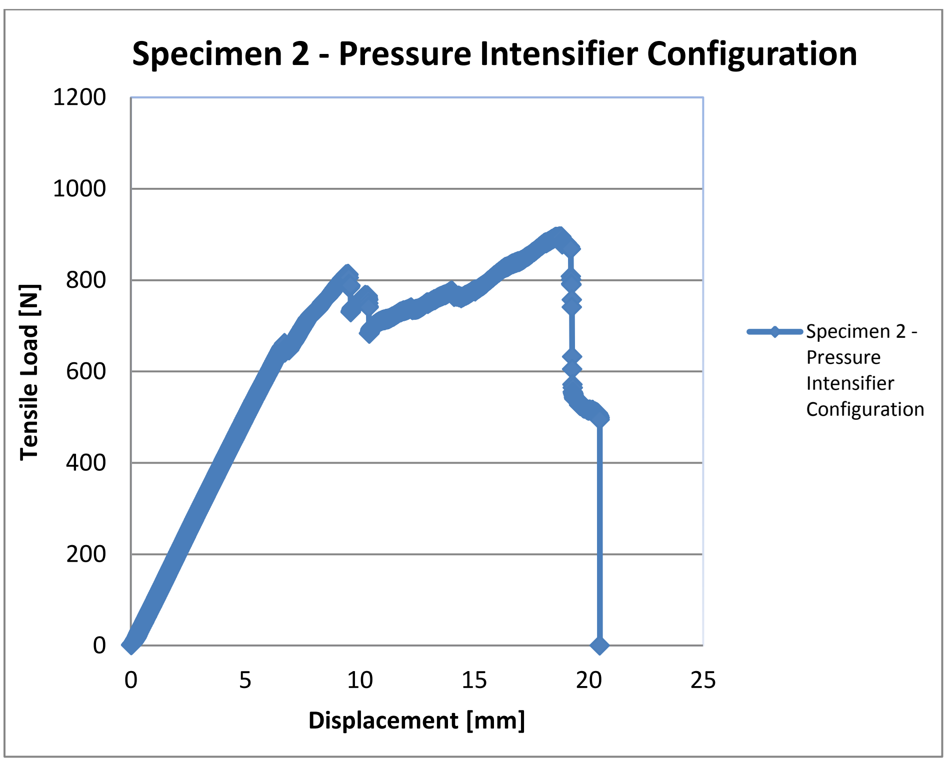

Figure 75 Load-displacement curve for Pressure Intensifier specimen 2

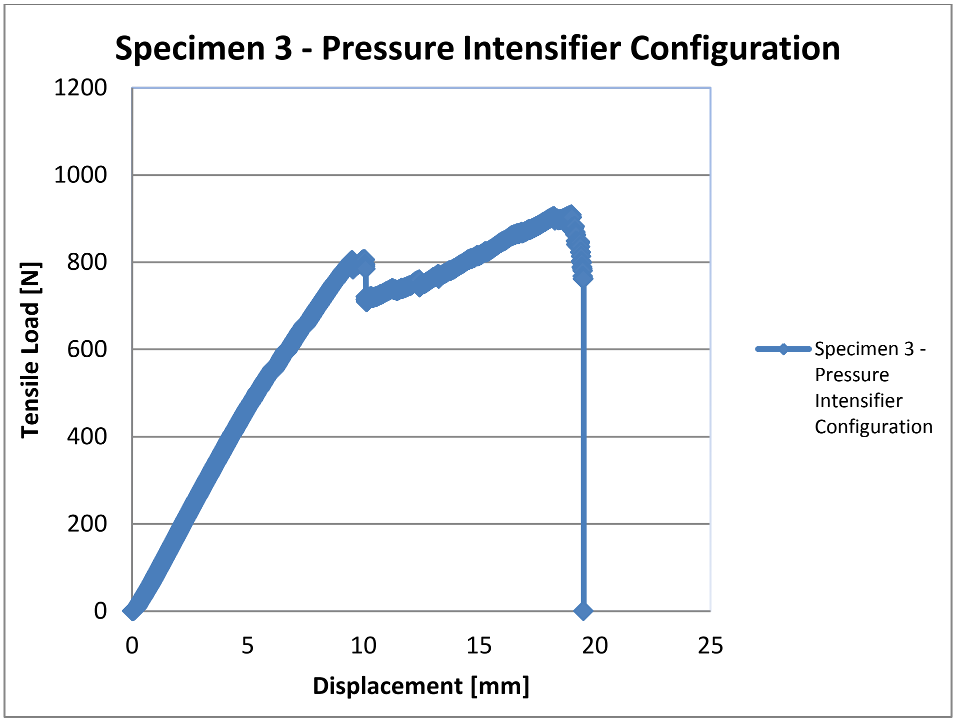

Figure 76 Load-displacement curve for Pressure Intensifier specimen 3

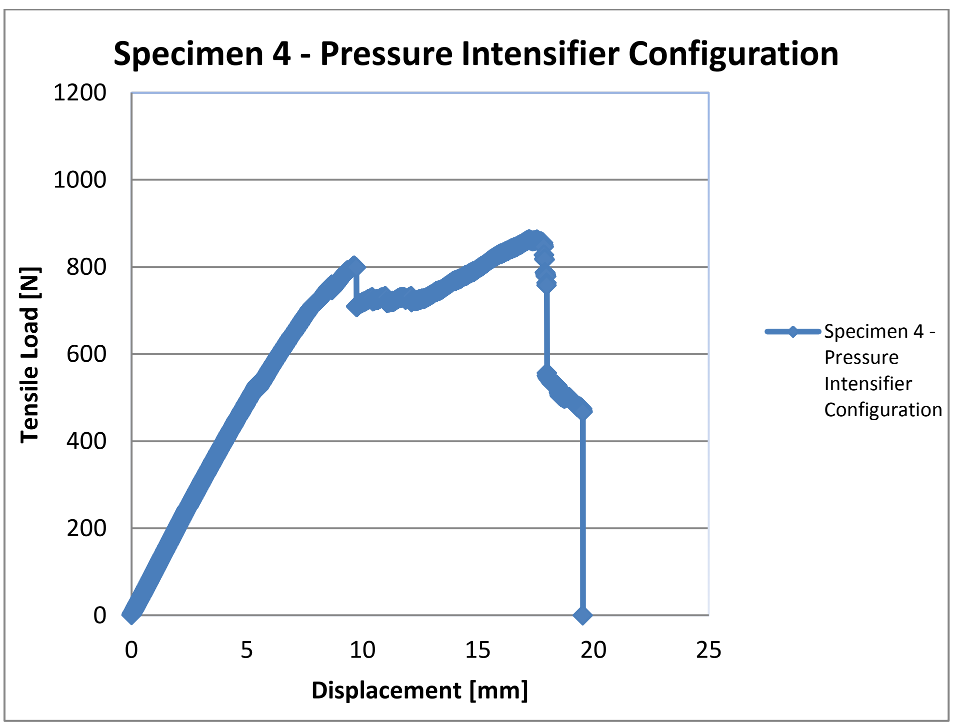

Figure 77 Load-displacement curve for Pressure Intensifier specimen 4

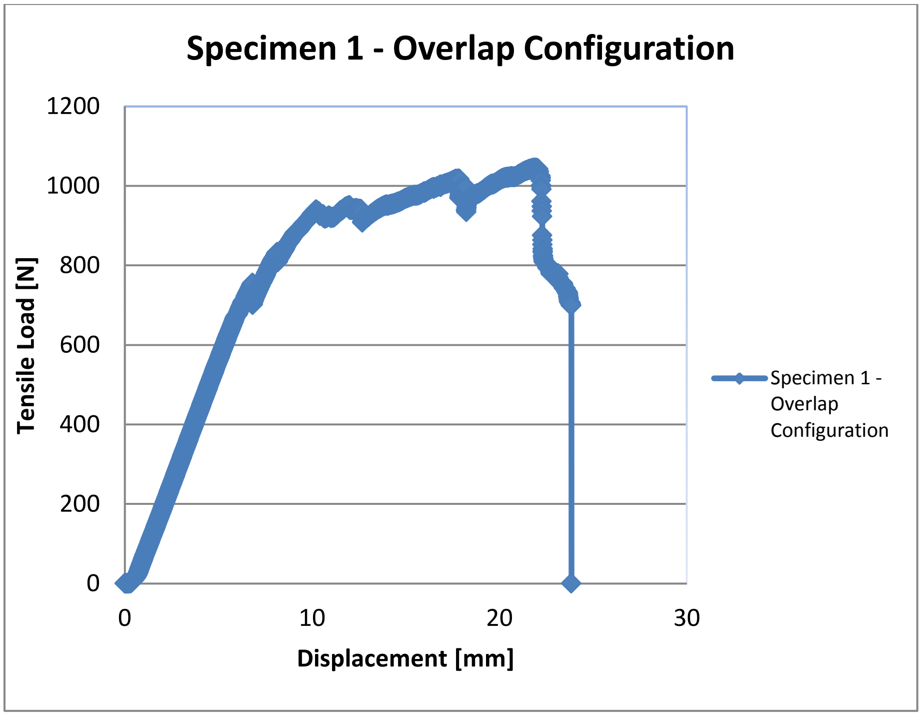

Figure 78 Load-displacement curve for Overlap specimen 1

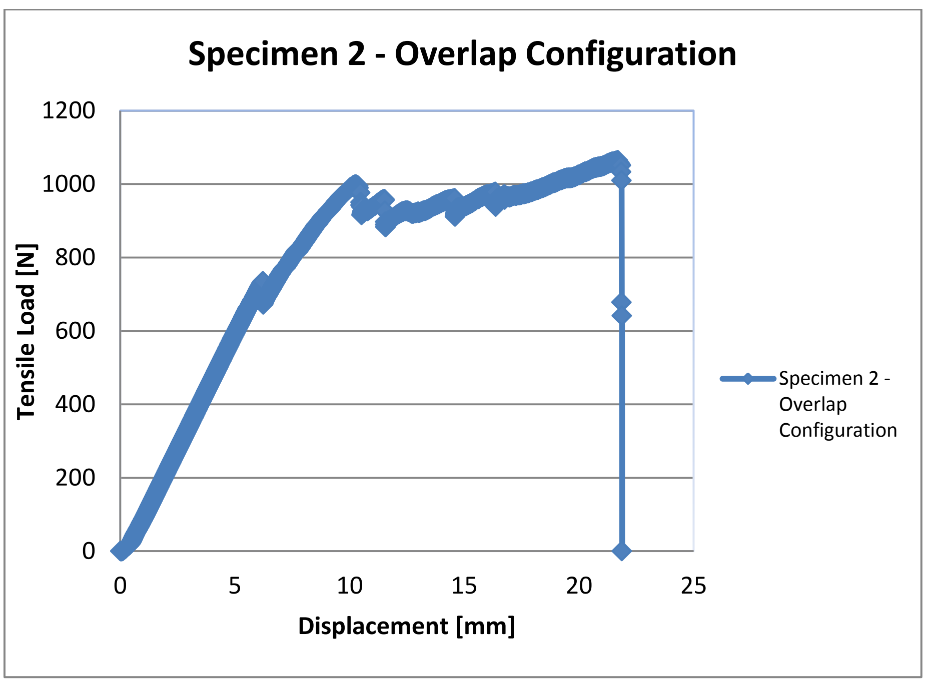

Figure 79 Load-displacement curve for Overlap specimen 2

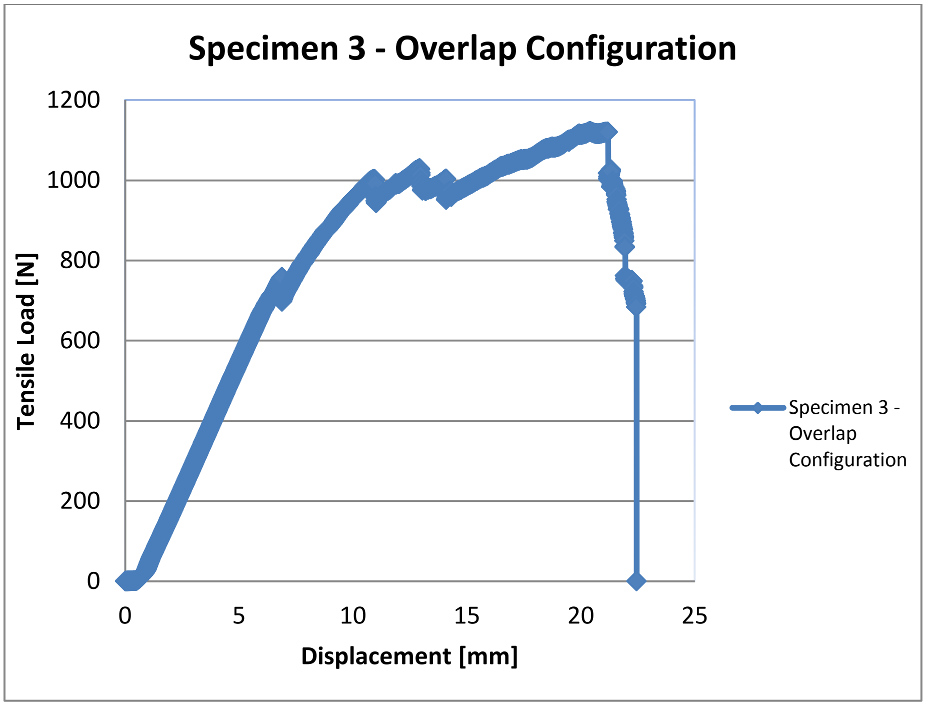

Figure 80 Load-displacement curve for Overlap specimen 3

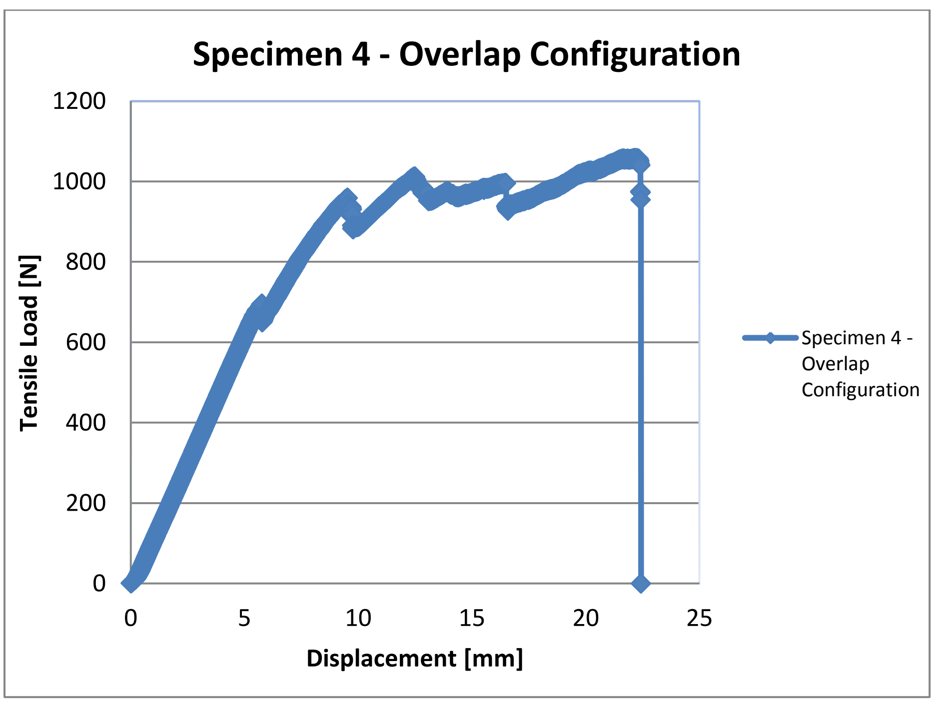

Figure 81 Load-displacement curve for Overlap specimen 4

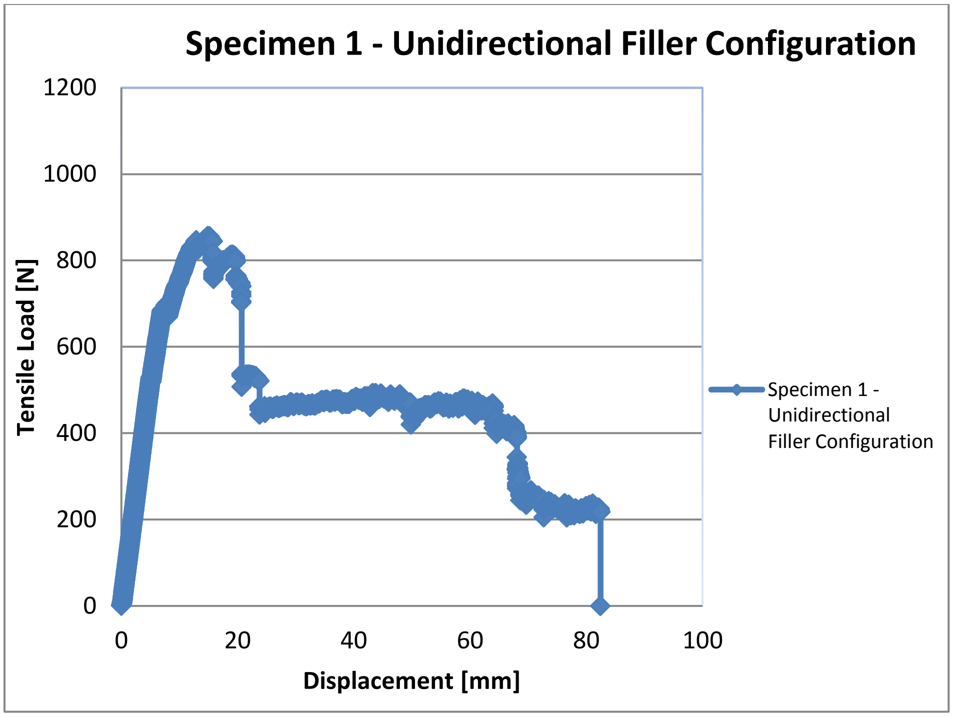

Figure 82 Load-displacement curve for Unidirectional Filler specimen 1

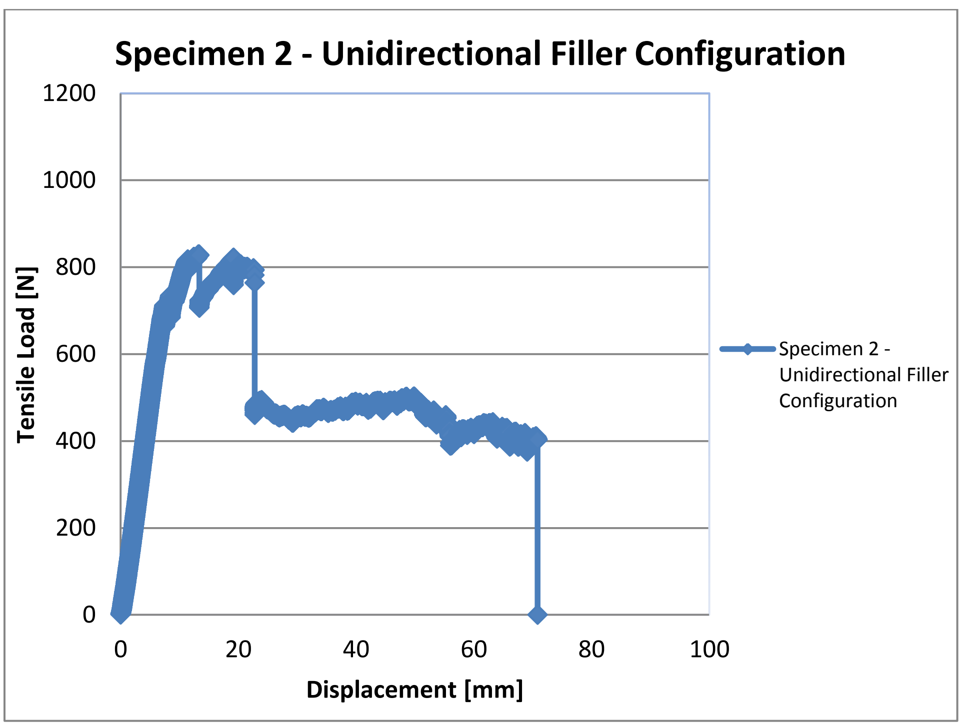

Figure 83 Load-displacement curve for Unidirectional Filler specimen 2

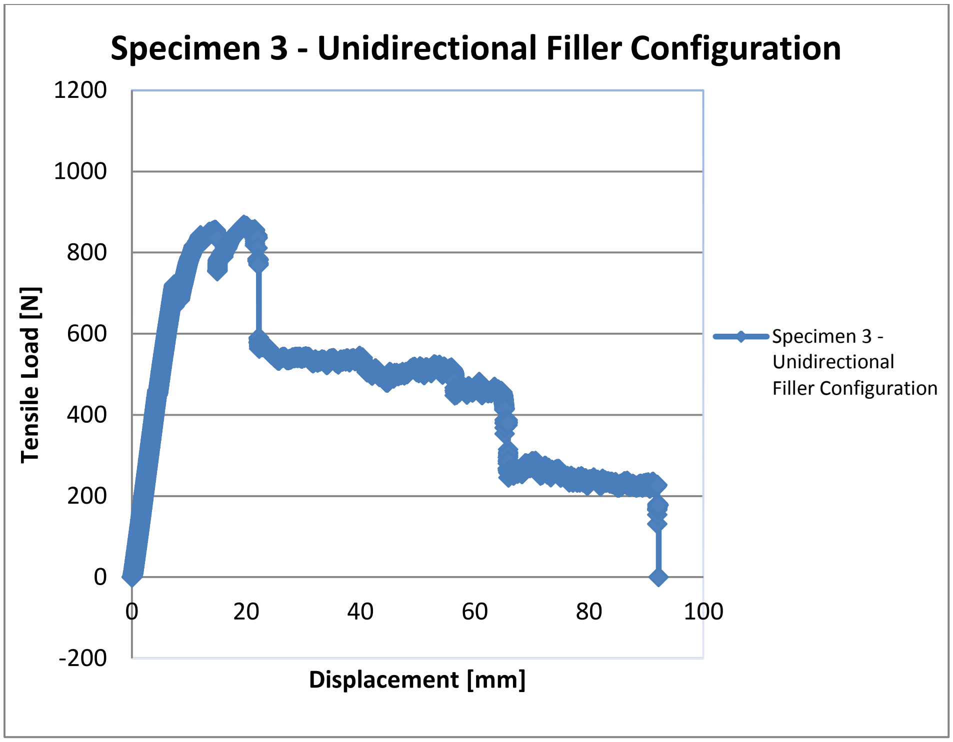

Figure 84 Load-displacement curve for Unidirectional Filler specimen 3

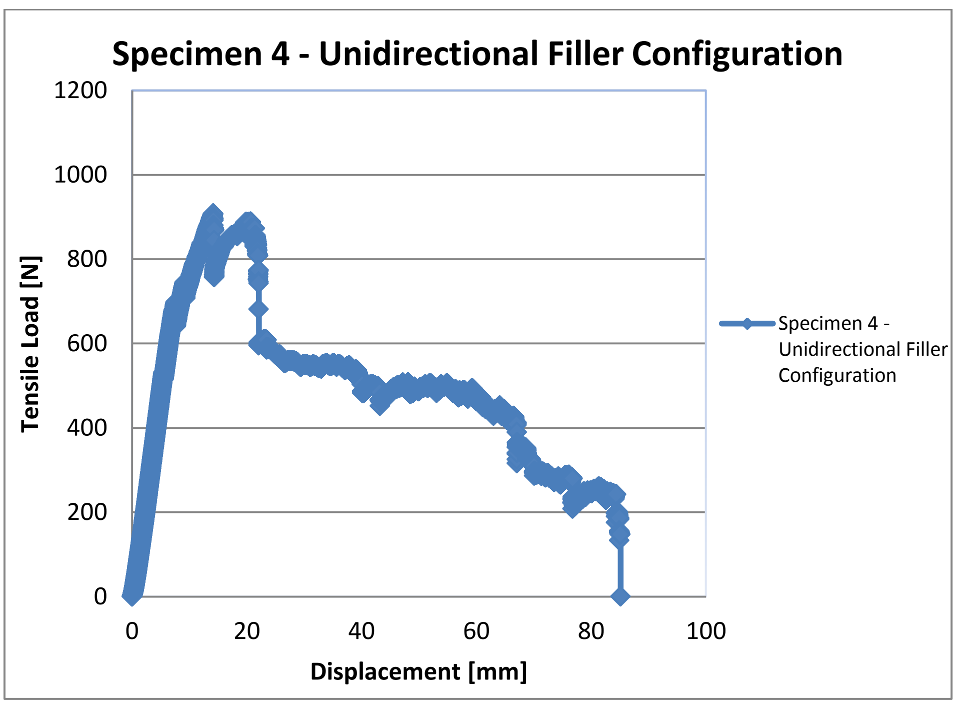

Figure 85 Load-displacement curve for Unidirectional Filler specimen 4